Direct Synthesis of Dimethyl Ether from Carbon Dioxide on a Physical Mixture of CuO-ZnO-Al_2O_3 and MCM-41-Supported Tungstophosphoric Acid

by

Betül Şeker

A Dissertation Submitted to the
Graduate School of Sciences and Engineering
in Partial Fulfillment of the Requirements for
the Degree of

Master of Science
in
Chemical and Biological Engineering

September 2019

Koç University

Graduate School of Sciences and Engineering

This is to certify that I have examined this copy of a master's thesis by

Betül Şeker

and have found that it is complete and satisfactory in all respects,
and that any and all revisions required by the final
examining committee have been made.

Committee Members:

_____

Assoc. Prof. Alper Uzun (Advisor)

_____

Prof. Ahmet Erhan Aksoylu

_____

Prof. Seda Keskin Avcı

Date: _____

ABSTRACT

Carbon dioxide (CO_2) plays an important role in the natural carbon cycle. However, increase in CO_2 emissions causes global warming and climate changes because of the so-called 'greenhouse effect'. Therefore, the chemical recycling of CO_2 to alternative fuels offers a prospective solution for these environmental concerns and provides new opportunities for sustainable future. In this view, conversion of CO_2 into liquid fuels is a promising approach. Among possible alternative products, such as methanol, hydrocarbons, and dimethyl ether (DME), DME can be used as an intermediate to produce several value-added products or as an alternative fuel. And it is the simplest ether without any C–C bonds; it is a colorless, nontoxic, and environmentally friendly. Because of its similar physical and chemical properties, it has a potential of substituting liquid petroleum gas (LPG). Besides, it is considered as a prospective future synthetic fuel owing to its high cetane number, more complete combustion, and low emission of toxic gases, such as SO_x, NO_x

The aim of this thesis is to develop an efficient catalyst for the conversion of CO_2 into DME. For this purpose, here, MCM-41-supported tungstophosphoric acid (TPA) and a commercial CuO-ZnO-Al_2O_3 methanol synthesis catalyst were physically mixed and the mixing ratios and reaction conditions were optimized for the highest DME production rate from CO_2 hydrogenation in a single-pass flow reactor. Data demonstrated that the highest DME space time yield was achieved at a TPA loading of 60 wt% in the TPA/MCM-41 catalyst and at a CuO-ZnO-Al_2O_3:TPA/MCM-41 mixing ratio of 4:1 using a gas hourly space velocity of 40 000 mL CO_2 g_{cat}^{-1} h^{-1} with an H_2:CO_2 ratio of 3:1 at 250 °C and 45 bar. At these conditions, the physical mixture provided a DME production rate of 1551.5 g_{DME} kg_{cat}^{-1} h^{-1}, to the best of our knowledge, is more than twice of the rate reported previously as the highest rate for DME production from CO_2 hydrogenation in a single-pass. Data suggested that this high performance was originated from the high density of acid sites in TPA/MCM-41 catalyst owing to exceptionally high surface area of MCM-41 offering a monolayer dispersion of TPA clusters even at a TPA loading of 60 wt%. Having a high density of acid sites in the physical mixture with a methanol synthesis catalyst offers a high efficiency in subsequent conversion of methanol into DME in a single pass reactor. Considering that this high DME production rate was obtained in a physical mixture containing a commercial methanol synthesis catalyst, optimized specifically for synthesis gas, results of this thesis present a broad potential of

TPA/MCM-41 solid acid catalysts for single-pass DME production from CO_2 hydrogenation, when used together with a methanol synthesis catalyst specifically designed for CO_2 hydrogenation.

ÖZET

Karbon dioksit (CO_2) doğal karbon döngüsünde önemli bir rol oynamaktadır. Ancak, CO_2 emisyonlarındaki artış, 'sera etkisi' denilen küresel ısınmaya ve iklim değişikliğine neden olmaktadır. Bu nedenle, CO_2'in alternatif yakıtlara ve katma değeri yüksek kimyasallara geri dönüşümü bu çevresel kaygılar için ileriye dönük bir çözüm sunmakla birlikte sürdürülebilir gelecek için yeni fırsatlar da sunmaktadır. Bu kapsamda CO_2'in sıvı yakıtlara dönüşümü umut verici bir yaklaşımdır. Bu yöndeki ilk çalışmalar metanol sentezi üzerine gerçekleştirilmiştir. Yakın zamanda metanolün hibrit sistemler kullanılarak olefinlere, aromatiklere, yüksek hidrokarbonlara ve dimetil etere (DME) dönüşümü üzerine çalışmalar yürütülmektedir. Bu ürünler arasında DME hem alternatif bir yakıt hem de yüksek katma değerli kimyasallar üretmek için bir ara ürün olarak kullanılması büyük bir avantaj sunmaktadır. C-C bağı olmayan bu en basit eter, renksiz, toksik olmayan çevre dostu bir üründür. Benzer fiziksel ve kimyasal özellikleri nedeniyle, sıvı petrol gazı (LPG) katkı malzemesi olarak kullanılma potansiyeline sahiptir. Ayrıca, yüksek setan sayısı, daha fazla yanma ve SO_x, NO_x gibi düşük toksik gaz emisyonları gibi özellikleri nedeniyle gelecekte kullanılabilecek sentetik bir yakıt olarak kabul edilmektedir.

Bu tez çalışmasında, CO_2'in DME'e dönüştürülmesi için etkili bir katalizör sistemi geliştirilmiştir. Bu amaçla, MCM-41 destekli tungstofosforik asit (TPA) ve ticari CuO-ZnO-Al_2O_3 metanol sentezi katalizörü ile fiziksel olarak karıştırılıp tek geçişli bir akış reaktöründe en yüksek DME üretim hızı için karışım oranları ve reaksiyon koşulları optimize edilmiştir. Elde edilen veriler ile en yüksek DME üretim hızının elde edilmesi için TPA/MCM-41 asit katalizöründe ağırlıkça %60'lık bir TPA yüklemesi ile 4:1'lik bir CuO-ZnO-Al_2O_3:TPA / MCM-41 fiziksel karışım oranında elde edilmesi gerektiği ve bu katalizörün 250 °C ve 45 bar altında H_2:CO_2 3:1 besleme oranı ile 40 000 mL CO_2 g_{cat}^{-1} $saat^{-1}$ akış test koşulları altında gerçekleştirilmesi gerektiği saptanmıştır. Optimize edilen reaksiyon koşulları altında elde edilen katalizör ile 1551.5 g_{DME} kg_{kat}^{-1} $saat^{-1}$ DME üretim hızı sağlamıştır. Elde edilen veriler, bu yüksek performansın, %60'lık bir TPA yüklemesinde TPA kümelerinin önemli derecede yüksek yüzey alanına sahip MCM-41 üzerinde tek tabakalı bir dağılımına imkan sunmasıyla TPA/MCM-41 katalizöründeki yüksek asit bölgesi yoğunluğundan kaynaklandığını göstermektedir. Bu yüksek DME üretim hızının, özellikle sentez gazı için optimize edilmiş ticari bir metanol sentezi katalizörü içeren fiziksel bir karışımda elde edildiğini göz önüne

alarak, sonuçlarımız özellikle CO_2 hidrojenlemesi için tasarlanmış bir metanol sentezi katalizörü ile birlikte kullanıldığında CO_2 hidrojenlemesinden tek geçişli DME üretimi için TPA/MCM-41 katı asit katalizörü kullanımına yönelik büyük bir potansiyel sunmaktadır.

ACKNOWLEDGMENTS

Firstly, I would like to thank my thesis advisor Assoc. Prof. Alper Uzun. His door was always open for me whenever I ran into a trouble in my research and I was always impressed that he always found a practical solution to the problems. Although I just spent 3 years as a master student, my story in Uzun Lab began at 2014. Therefore, I would like to thank him one more time for providing to me take part in KUTEM family again. Also, I will never forget that he always supported me after each English test results. It has been a great opportunity for me to work with him.

I want to express my sincere thanks to my thesis committee members Prof. Ahmet Erhan Aksoylu and Prof. Seda Keskin Avcı.

My sincere thanks got to Turkish Petroleum Refineries Corporation (TÜPRAŞ) and Koç University TÜPRAŞ Energy Center (KUTEM) for providing support and giving me the opportunity to work on this project. I would like to thank Ersen Ertaş and Deniz Onay Atmaca and I also thank Dr. Melek Selcen Başar for her supports and motivation throughout the project and business life.

There is no way to express how much it meant to me to have been a member of Uzun Lab. My special thanks go to KUTEM girls, Dr. Melike Babucci, Samira Fatma Kurtoğlu, Dr. Özge Deniz Bozkurt, Özge Akarçay, and Elif Kocaman without them I would not have found motivation when I was coping with my work problems. I also thank Dr. Ahsan Jalal not only for his support and valuable advices but also for working together on weekends and always opening my reactors and regulators. I would like to also thank Vahid Nozari, Muhammad Zeeshan, and Tolga Koçer. I am also very thankful to Volkan Balci for his help in the beginning of this thesis study.

My special thanks to Işık Sena Akgün and Buket Yüksel for listening, offering me advice, and supporting me through this entire process. They were always with me.

Finally, there are no proper words to convey my deep gratitude to my family. This journey would not have been possible without their continuous love, help, and support. I am especially grateful to my mom Sultan Şeker, thank you for encouraging me to follow my dreams. She is the most powerful women in the world. Also, I am very lucky because I have three best friends Ayşegül Şeker, Gökçe Nur Şeker, Merve Nur Şeker and I know they will always be my best friends till the end of the life. I am forever indebted to my dad Ercan Şeker for giving opportunities to make me who I am now. Also, I want to thank my granny for her advice and continuous support. I always knew that they believed in me and they wanted the best for me. Thank you for everything… I dedicate this milestone to them…

Sultanım'a

TABLE OF CONTENTS

LIST OF TABLES

LIST OF FIGURES

NOMENCLATURE

GHG	=	Greenhouse Gas
CO_2	=	Carbon Dioxide
MeOH	=	Methanol
CO	=	Carbon Monoxide
DME	=	Dimethyl Ether
Ar	=	Argon
O_2	=	Oxygen
N_2	=	Nitrogen
CH_4	=	Methane
TPA	=	Tungstophosphoric Acid
MCM-41	=	Mobil Composition of Matter No. 41 Mesoporous Silica
HPA	=	Heteropoly Acid
MicroGC	=	Micro Gas Chromatography
XRD	=	X-ray Diffraction
FTIR	=	Fourier Transform Infrared Spectroscopy
NH_3-TPD	=	Ammonia Temperature Programmed Desorption
TCD	=	Thermal Conductivity Detector
BET	=	Brunauer-Emmett-Teller
BJH	=	Barrett-Joyner-Halenda
XRF	=	X-Ray Fluorescence
TGA	=	Thermogravimetric Analysis
RWGS	=	Reverse Water Gas Shift
GHSV	=	Gas Hourly Space Velocity
STY_{DME}	=	Space Time Yield of Dimethyl Ether
X_{CO2}	=	Conversion of Carbon dioxide
$S_{product}$	=	Selectivity of Product

Chapter 1

INTRODUCTION

Carbon dioxide, which causes global warming and climate change, is known as the primary responsible gas for greenhouse effect. In this regard, to reduce the CO_2 emissions the Intergovernmental Panel on Climate Change (IPCC) and the United Nations Conference on Climate Change (COP21, Paris, 2015) highlighted the need of precaution by at least half of the current value by 2050 with the aim of limiting the global average temperature increase to at least of 2 °C [1].

Reducing CO_2 emissions is a long and comprehensive job. In this respect, there are three possible feasible strategies; reduction of CO_2 amount produced, storage of CO_2, and usage of CO_2 [2,3]. As a first strategy, less carbon contain energy is needed for energy efficient improvements by shifting from fossil fuels to renewable energy [4, 5]. CO_2 storage is the second approach which includes the new development of capture methods [6-9]. In addition to these, as a third approach, hydrogenation reaction has been recognized during many years as one of the most significant chemical conversions of CO_2; it also provides a great possibility for sustainable energy [10, 11]. In this view, the conversion of CO_2 into liquid fuels is a promising approach. Among possible alternative products, such as methanol (MeOH), hydrocarbons, and dimethyl ether (DME), DME can be used as an intermediate to produce several value-added products or as an alternative fuel.

Hydrogenation of CO_2 into DME has gained a tremendous attention in this regard, because DME offers a good prospect both as an alternative fuel and as an intermediate for the production of several value-added products (gasoline, aromatics, and olefin). DME is the simplest ether and it is not toxic or carcinogenic molecule. It has a boiling point of -25 °C, however it can be liquefied at room temperature under a pressure of approximately 0.5 MPa [12]. Its chemical and physical properties are similar to liquid petroleum gas (LPG) so it can be blended with LPG [13]. In addition to this, DME has also been recognized as an auto transportation fuel alternative to diesel fuel owing to its physicochemical properties like high cetane number, lower auto-ignition temperature, low-emission of NO_x, SO_x etc.

DME production, however, usually requires a two-step process, where methanol produced over metallic-based catalyst in the first step, then methanol is dehydrated to yield DME on a solid acid catalyst, such as zeolites or alumina. For the direct synthesis of DME, the catalyst functionalities of CO_2 activation for methanol synthesis and *in-situ* dehydration step are integrated using multifunctional systems. Currently, several investigations are now focusing on using zeolites for the methanol dehydration step. However, heteropoly acids can be good candidates for this purpose. Heteropoly acids, particularly Keggin-type-heteropoly acids, has drawn a growing attention in a class of solid acids because of their intrinsic characteristics such as high Bronsted acidity, excellent redox stability, and environmentally friendly properties which make them promising catalysts for acid-catalyzed reactions [14]. In this study, our aim is to assess the potential of heteropoly acids (HPAs), particularly Keggin-type-heteropoly acids, as the acid function of the physical mixture for the direct conversion of CO_2 into DME.

The research described in this dissertation focuses on the development of an efficient catalyst for the conversion of CO_2 into DME. For this purpose, the commercial MeOH synthesis catalyst, $CuO\text{-}ZnO\text{-}Al_2O_3$, was mixed with a solid acid catalyst, made of mesoporous silica supported heteropoly acids, as a physical mixture and considered for the serial conversion of CO_2 first into MeOH on the methanol synthesis catalyst and then to DME on the solid acid catalysts upon a single-pass in the reactor using direct DME synthesis. The paragraphs below set out the content of the chapters that follow.

Chapter 2 comprises of a literature review on CO_2 emission, strategies for the reduction of CO_2, which include carbon capture storage and carbon capture utilization processes, and dimethyl ether fuel properties and its applications.

Chapter 3 provides a literature review on CO_2 hydrogenation reactions for direct and indirect dimethyl ether synthesis and catalysts for CO_2-to- MeOH and MeOH dehydration processes.

Chapter 4 introduces the experimental component of the investigation, including sample preparation techniques, characterization methods, and catalytic testing system details that were used in this study.

Chapter 5 presents the detailed characterization of various mixing of MeOH synthesis catalyst and solid acid catalyst samples. Also, this chapter reports the consequences of changing of MeOH synthesis catalyst and solid acid catalyst ratio, TPA loading of solid acid catalyst and

reaction conditions, such as temperature and GHSV on their catalytic performances of them for DME production under CO_2 hydrogenation conditions.

Chapter 6 concludes with future directions and outlook of this thesis.

The most significant finding of this thesis is that the physical mixture of the catalysts considered here provides a record high DME production rate, offering opportunities for further improvement of this rate by the application of this concept of using mesoporous silica supported heteropoly acids as the acid component of the physical mixture to other methanol synthesis catalysts specifically designed for CO_2 hydrogenation

References

[1] P. Zhou, M. Wang, Carbon dioxide emissions allocation: A review, Ecological Economics, 125 (2016) 47-59.

[2] M. Mikkelsen, M. Jørgensen, F.C. Krebs, The teraton challenge. A review of fixation and transformation of carbon dioxide, Energy Environ. Sci., 3 (2010) 43-81.

[3] S.K. Hoekman, A. Broch, C. Robbins, R. Purcell, CO_2 recycling by reaction with renewably-generated hydrogen, International Journal of Greenhouse Gas Control, 4 (2010) 44-50.

[4] M. Soltanieh, K.M. Azar, M. Saber, Development of a zero emission integrated system for co-production of electricity and methanol through renewable hydrogen and CO_2 capture, International Journal of Greenhouse Gas Control, 7 (2012) 145-152.

[5] A. Talebian-Kiakalaieh, N.A.S. Amin, H. Mazaheri, A review on novel processes of biodiesel production from waste cooking oil, Applied Energy, 104 (2013) 683-710.

[6] L. Han, Q. Wang, Z. Luo, N. Rong, G. Deng, H_2 rich gas production via pressurized fluidized bed gasification of sawdust with in situ CO_2 capture, Applied Energy, 109 (2013) 36-43.

[7] J. Wang, V. Manovic, Y. Wu, E.J. Anthony, A study on the activity of CaO-based sorbents for capturing CO_2 in clean energy processes, Applied Energy, 87 (2010) 1453-1458.

[8] J.M. Valverde, P.E. Sanchez-Jimenez, A. Perejon, L.A. Perez-Maqueda, Constant rate thermal analysis for enhancing the long-term CO2 capture of CaO at Ca-looping conditions, Applied Energy, 108 (2013) 108-120.

[9] B. Li, Y. Duan, D. Luebke, B. Morreale, Advances in CO_2 capture technology: A patent review, Applied Energy, 102 (2013) 1439-1447.

[10] W.M. Budzianowski, Value-added carbon management technologies for low CO_2 intensive carbon-based energy vectors, Energy, 41 (2012) 280-297.

[11] W. Wang, S. Wang, X. Ma, J. Gong, Recent advances in catalytic hydrogenation of carbon dioxide, Chemical Society Reviews, 40 (2011) 3703-3727.

[12] C. Arcoumanis, C. Bae, R. Crookes, E. Kinoshita, The potential of di-methyl ether (DME) as an alternative fuel for compression-ignition engines: A review, Fuel, 87 (2008) 1014-1030.

[13] T. Ogawa, Direct Dimethyl Ether Synthesis, Journal of Natural Gas Chemistry 12 (2003) 219-227.

[14] I. V. Kozhevnikov, Catalysis by Heteropoly Acids and Multicomponent Polyoxometalates in Liquid-Phase Reactions , Chemical Reviews, 98 (1998) 171-198.

Chapter 2

LITERATURE REVIEW ON CARBON DIOXIDE EMISSIONS, STRATEGIES FOR REDUCTION OF CARBON DIOXIDE AND DIMETHYL ETHER AS AN ALTERNATIVE FUEL

2.1 Carbon Dioxide Emissions

In today's world, increasing population and economic growth bring an increase in global energy consumption as well. Currently, fossil fuels such as coal, gas, and oil are the major energy sources and dominate encompassing between 80 to 90 percent of total energy consumption. The International Energy Outlook 2019 (IEO2019) project by the U.S. Energy Information Administration expect to increase global energy usage by 28 percent between 2015 and 2040. While IEO2019 expects non-fossil fuels such as renewables or nuclear fuels to grow quicker than fossil fuels, fossil fuels still account for over three-quarters of global total energy consumption by 2040 [1]. Fuels are based on hydrocarbons and energy production from fossil fuels by burning hydrocarbons accounts for the greenhouse gas (GHG) emissions, capable of absorbing and emitting thermal radiation in the Earth's atmosphere and greenhouse gas mainly consist of CO_2 of nearly 75%. Cement and steel production industries along with vehicles, and coal-based power plants are considered as the main sources of CO_2 emission [2]. Compared to other fossil fuels, CO_2 emissions from power plants are associated with elevated coal consumption, which has the largest carbon content per unit of energy produced.

The CO_2 concentration in the atmosphere remained stable until the late 17^{th} century. After that, CO_2 emissions have been growing since pre-industrial time and CO_2 concentration is increasing constantly from 280 ppm (parts per million) before the industrial revolution in the mid-1800s to 412 ppm in 2019 recently, and CO_2 average growth is 2 ppm/year in the last 10 years [3-5]. The change in CO_2 concentration over the past 1000 years is summarized in Table 2.1 [6].

Table 2.1 Change in CO_2 concentration of last 1000 years [6].

CO_2 concentration (ppm)	Year	Period (year)	Increase (ppm)
270-280	1000-1800	800	10
280-310	1800-1950	150	30
315-330	1958-1973	15	15
330-380	1973-2006	33	50
380-412	2006-2019	13	32

That much increasing in CO_2 emissions at the atmosphere causes global warming and climate changes. Also, despite their considerable size, fossil fuel reserves are limited. Therefore, the chemical recycling of CO_2 to alternative fuels offers a prospective solution both for environmental concern and fossil fuel depletion [7-9].

2.2 Strategies for Reduction of Carbon Dioxide

To discover alternatives to reduce greenhouse gas emissions, it is essential to know worldwide driving factors of CO_2 emissions. A need for more sustainable development has been developed by increasing social awareness of environmental issues. CO_2 emissions are growing with every year. Such high emissions forced governments to implement CO_2 emissions reduction strategies [10].

The Intergovernmental Panel on Climate Change (IPCC) and the International Climate Agreement, which is the United Nations Conference on Climate Change (COP21) hold on in Paris in December 2015 have emphasized the need for reducing the CO_2 emissions. According to this agreement, the aim is to keep the global temperature increase within a maximum of 2 °C so this would significantly reduce risks the impacts of climate change [10].

During the last decades, several strategies and technologies have been developed concerning capture and storage of carbon dioxide (CCS) and, capture and utilization (CCU) of carbon dioxide [11]. The negative environmental impact associated with burning fossil fuels has brought economic and scientific interest to reduce CO_2 emissions as well.

2.2.1 CO_2 Capture and Storage (CCS)

Continuous progress has been made in the technology of CO_2 capture over the past decades [12]. Power plants, refineries and several large-scale iron, steel, and cement manufacturing plants are the primary targets for the enforcement of the capture techniques. The methods of CO_2 capture and separation are widely split into physical and chemical processes like absorption, membrane adsorption or chemical looping.

For industrial scale application, enhanced oil recovery is the most popular technique. Using this method, CO_2 can be injected into oil wells to move oil out of the wells and oil can be recovered [13]. The storage of captured CO_2 in empty oil areas is an alternative storage technique. However, it needs special care because of any accidental leakage and apart from the technical difficulties, it needs a considerable amount of financial investment.

2.2.2 CO_2 Capture and Utilization (CCU)

Capture and utilization technology are used for CO_2 to create crucial products. The most beneficial method is that if CO_2 captured from the sources is utilized in an energy efficient manner, the global warming impact of many of high economic value processes will be minimized. In addition, hydrogenation reaction has been verified for many years as one of the most significant chemical conversions of CO_2; it also provides a sustainable development in the energy and environmental industries. Indeed, the hydrogenation method not only decreases the growing quantity of CO_2 in the atmosphere but also results in fuels and valuable chemicals being produced [14]. However, because of the high thermodynamic and kinetic stability of CO_2, it was not used with its fullest potential until today [15, 16]. That's why, using efficient catalyst and selective pathways are necessary to get high production rate of desired products. In this view, many research activities are focusing on the development of these new catalytic technologies, one of them is the conversion of CO_2 into liquid fuels, which is a very promising approach. And the transformation of CO_2 into chemicals and fuel-alternatives or fuel additives would be an excellent option to achieve large scale CO_2 reduction. For example, CO_2 can be converted into chemicals and fuels by the reduction of synthesis gas, MeOH, urea, polycarbonate etc. Since fuel market demand is higher than organic chemicals, catalytic conversion of CO_2 to fuels, instead of organic chemicals, will play a significant role in policies to manage CO_2 emission. In addition, CO_2 emissions are mainly connected with fossil fuel

consumption, so CO_2-synthesized fuels can replace the fossil fuels and help to close the open carbon cycle. CO_2 can be utilize for the production of fuels, by reverse water gas shift reaction (RWGS) and subsequent Fischer-Tropsch synthesis. For example, like this path CO_2 conversion to methanol is a promising approach because methanol is a platform molecule for various valuable chemicals, such as DME which can act as a fuel itself as well. Recently, DME production from CO_2 using MeOH dehydration process is getting attention because of its numerous fuel properties, which are more described in Chapter 2.3.

2.3 Dimethyl Ether as an Alternative Fuel

2.3.1 Dimethyl Ether Properties

DME is the simplest ether having a chemical formula of CH_3OCH_3 without any C–C bonds and it is also known as methoxy methane. It is non-toxic, non-carcinogenic [17], colorless, and volatile organic compound. It is in gas form at standard temperature and pressure. Its other physical properties are summarized in Table 2.2. Like liquefied petroleum gas (LPG), it can be stored and transported easily since it can be liquefied at 5 bar or -25 °C [18].

Table 2.2 Properties of dimethyl ether [17,18].

Properties	
Chemical Structure	CH_3OCH_3
Molecular weight (g mol^{-1})	46
Liquid density (g cm^3)	0.67
Vapor pressure (bar)	5.3
Cetane number	55-60
Boiling point (°C)	-24.9
Carbon Content (wt%)	30.8
Heat of Evaporation (kJ mol^{-1})	21.5

2.3.2 Applications of Dimethyl Ether

Currently, DME has many applications, with tremendous attention from both the industry and the academia. Especially, it can be used as a fuel and it can be used for the manufacturing of chemical products as a chemical intermediate. Its applications are mentioned briefly below.

DME is considered as a non-petroleum based clean compression ignition fuel. After the beginning of 1980's it has been used as an additive for ignition aid in diesel engines [18]. Unlike other transportation fuels, such as diesel, DME can be considered as environmentally friendly. Because of its high oxygen content (35 %), soot formation is reduced. Also, there is no nitrogen and sulfur content compounds, so it produces no SO_x and NO_x emissions after burning. In addition to this, in the atmosphere, DME can be easily decomposed into CO_2 and H_2O, which make it so attractive as an environmentally friendly fuel. Cetane number, an indication of the combustion quality of diesel fuel, is around 60 for DME which is relatively higher than that of diesel [19-21]. However, the only drawback of it, because of the lower heating values, approximately 1.5 times volume of DME is required to meet the same amount of heating value for diesel. DME engines and vehicles development have already been completed and tested in China and Sweden. For example, Volvo Trucks fueled by DME in 2013 and very recently Ford Motor Company introduced world's first production passenger car which is powered fully by DME in 2019.

DME can also be used as a chemical feedstock and an intermediate for the production of value-added products, such as light olefins [22], propylene[22], methyl acetate[23, 24], acetic acid, formaldehyde, dimethyl sulphate, and gasoline [25].

Also as a substitute fuel properties, DME can be used for electric power generation and it can be used for domestic heating and cooking purposes as well [26]. Thanks to its similar LPG like properties, DME can be blended with LPG up to 50 vol.% with only a slight decrease in thermal efficiency and DME can reduce LPG consumption for cooking and heating purposes [27].

Apart from its fuel properties, DME can also be used as aerosol propellant. Decomposition of DME in the atmosphere takes place very easily and has no concern over ozone layer depletion, so it can be a good alternative to harmful chloro-fluoro carbons, which

are using for propellant applications recently. With this property, DME can also be used in cosmetic industry for hair sprays, deodorants, antiperspirant, and in various spray cans as well.

References

[1] International Energy Outlook 2018 (Jan. 24, 2019) access on August 11, 2019

[2] IPCC 2005, Sources of CO_2, in: B. Metz, Davidson, O., de Conick, H.C., Loos, M., Meyer L.A., (Ed.) PCC Special Repost on Carbon Dioxide Capture and Storage. Prepared by Working Group III of the Intergovernmental Panel on Climate Change, Cambridge, United Kingdom and New Your, NY, USA, 2005, pp. 75-103.

[3] (IEA) International Energy Agency, Key Trends in CO_2 emissions, CO_2 emissions from fuel combustion Paris, France, 2015.

[4] D. M. Etheridge, L. P. Steele, R. L. Langenfelds, R. J. Francey, J.-M. Barnola, V. I. Morgan, J. Geophys. Res. Atmosphere, 101 (1996) 4115–4128.

[5] D. Lüthi, M. Le Floch, B. Bereiter, T. Blunier, J.-M. Barnola, U. Siegenthaler, D. Raynaud, J. Jouzel, H. Fischer, K. Kawamura, T. F. Stocker, Nature 453 (2008) 379–382.

[6] Global Greenhouse Gas Reference Network (2018, Oct 01) Retrieved from https://www.esrl.noaa.gov/gmd/ccgg/trends/index.html access on August 11, 2019.

[7] T.C. Johnson, D.J. Morris, M. Wills, Hydrogen generation from formic acid and alcohols using homogeneous catalysts, Chem Soc Rev, 39 (2010) 81-88.

[8] S. Enthaler, Carbon dioxide the hydrogen storage material of the future, ChemSusChem, 1 (2008) 801-804.

[9] C. Federsel State-of-the-Art Catalysts for Hydrogenation of Carbon Dioxide, Angewandte Chemie International Edition, 49 (2010), 6254-6257.

[10] United Nations Conference on Climate Change (COP21) Paris Climate Change Conference; Paris, France, (2015) Nov30–Dec 11. Retrieved from http://www.cop21.gouv.fr/en/, access on August 15, 2019.

[11] R.M. Cuéllar-Franca, A. Azapagic, Carbon capture, storage and utilisation technologies: A critical analysis and comparison of their life cycle environmental impacts, Journal of CO_2 Utilization, 9 (2015) 82-102.

[12] J. Gibbins, H. Chalmers, Carbon capture and storage, Energy Policy, 36 (2008) 4317-4322.

[13]Lake, L.W. Enhanced oil recovery, United States, p., 1989. https://www.osti.gov/biblio/5112525, access on August 15, 2019.

[14] W.M. Budzianowski, Value-added carbon management technologies for low CO_2 intensive carbon-based energy vectors, Energy, 41 (2012) 280-297.

[15] A. Alvarez, M. Borges, J.J. Corral-Perez, J.G. Olcina, L. Hu, D. Cornu, R. Huang, D. Stoian, A. Urakawa, CO_2 Activation over Catalytic Surfaces, Chemphyschem, 18 (2017) 3135-3141.

[16] C. Song, CO_2 Conversion and Utilization: An Overview. ACS Symposium Series; American Chemical Society: Washington, DC, 2002.

[17] Robust Summary for Dimethyl Ether; prepared by DuPont for the US EPA, Chemical Right to Know Program, 2000.

[18] C. Arcoumanis, C. Bae, R. Crookes, E. Kinoshita, The potential of di-methyl ether (DME) as an alternative fuel for compression-ignition engines: A review, Fuel, 87 (2008) 1014-1030.

[19] S.H. Park, C.S. Lee, Combustion performance and emission reduction characteristics of automotive DME engine system, Progress in Energy and Combustion Science, 39 (2013) 147-168.

[20] S. Xu, Y. Wang, X. Zhang, X. Zhen, C. Tao, Development of a novel common-rail type Dimethyl ether (DME) injector, Applied Energy, 94 (2012) 1-12.

[21] S.H. Yoon, J.P. Cha, C.S. Lee, An investigation of the effects of spray angle and injection strategy on dimethyl ether (DME) combustion and exhaust emission characteristics in a common-rail diesel engine, Fuel Processing Technology, 91 (2010) 1364-1372.

[22] T.-S. Zhao, T. Takemoto, N. Tsubaki, Direct synthesis of propylene and light olefins from dimethyl ether catalyzed by modified H-ZSM-5, Catalysis Communications, 7 (2006) 647-650.

[23] P. Cheung, A. Bhan, G. Sunley, D. Law, E. Iglesia, Site requirements and elementary steps in dimethyl ether carbonylation catalyzed by acidic zeolites, Journal of Catalysis, 245 (2007) 110-123.

[24] A. Bhan, Specificity of Sites within Eight-Membered Ring Zeolite Channels for Carbonylation of Methyls to Acetyls, Journal of American Chemical Society, 129 (2007), 4919-4924.

[25] G. Olah, Chemical Recycling of Carbon Dioxide to Methanol and Dimethyl Ether: From Greenhouse Gas to Renewable, Environmentally Carbon Neutral Fuels and Synthetic Hydrocarbons, Journal of Organic Chemistry, 74 (2009) 487–498.

[26] DME Handbook; Ohno, Y., Ed.; Japan DME Forum, 2007.

[27] R. Anggarani, C.S. Wibowo, D. Rulianto, Application of Dimethyl Ether as LPG Substitution for Household Stove, Energy Procedia, 47 (2014) 227-234.

Chapter 3

LITERATURE REVIEW ON REACTIONS AND CATALYSTS OF CARBON DIOXIDE HYDROGENATION FOR DIMETHYL ETHER SYNTHESIS

3.1 Carbon Dioxide Hydrogenation Reactions for Dimethyl Ether Synthesis

Basically, there are two main paths for the production of dimethyl ether (DME); an indirect two-step process and a direct one-step process. In the two-step process, firstly, methanol (MeOH) is synthesized from syngas over a metallic catalyst, then the methanol condensation occurs in a secondary step on an acid catalyst located in a different reactor. On the other hand, in the direct one-step process, multifunctional catalysts combining a metallic catalyst with an acid catalyst are used in only one reactor.

Conventionally, in two-step process, the synthesis of DME from syngas or pure carbon dioxide requires the combination of two different catalytic functions: selective hydrogenation of CO_2 to methanol and methanol dehydration into DME. Methanol is produced industrially from syngas which can be described by following equations which are exothermic and they both result in a stoichiometric decrease of total number of molecules, so they are thermodynamically limited and favored at low temperatures and high pressures;

Methanol synthesis: $CO_2 + 3H_2 \leftrightarrow CH_3OH + H_2O$ $\Delta H_{298\,K} = -49.5$ kJ mol^{-1} (Eq 3-1)

Methanol synthesis: $CO + 2H_2 \leftrightarrow CH_3OH$ $\Delta H_{298\,K} = -90.6$ kJ mol^{-1} (Eq 3-2)

Reverse water gas shift reaction: $CO_2 + H_2 \leftrightarrow CO + H_2O$ $\Delta H_{298\,K} = 41.2$ kJ mol^{-1} (Eq 3-3)

The dehydration of methanol into DME is a commercial route. The dehydration reaction takes place at a temperature range of 250 – 400 °C and at a pressure of 20 bar. After reaction takes place, at least two different columns are used for DME purification to remove water and unreacted methanol, if any. The reaction is limited by equilibrium and it is exothermic and equimolar with a standard enthalpy of -23.4 kJ/mol at 298 K.

Methanol dehydration: $2CH_3OH \leftrightarrow CH_3OCH_3 + H_2O \quad \Delta H_{298\,K} = -23.4$ kJ/mol (Eq 3-4)

The direct one-step process was admitted to the beginning of the 1990s because of the stringent requirements of environmental regulations. For this process, DME can be synthesized directly from syngas or pure CO_2 using multifunctional catalytic system that allows both methanol synthesis and methanol dehydration in a single reactor.

In recent years, the feasibility of using one-step process is getting more attention because of two main reasons. The first reason comes from the thermodynamic point of view. Indirect two-step method has higher thermodynamic limitations than the direct one-step process has. The MeOH consumption throughout the MeOH dehydration to DME reaction breaks the equilibrium and the reaction shifts to the right side [1]. MeOH synthesis form CO_2 is favored at low temperature and high pressure. Therefore, these restrictions can be reduced by producing DME at the same time with co-producing of it since the equilibrium constant of MeOH dehydration process is much higher than that of MeOH synthesis reaction [2] or another efficient way to by-pass it, is the continuous removal of MeOH from reaction system with physically. Using the MeOH synthesis and dehydration of MeOH process in tandem, the thermodynamics is compelled to shift towards the desired way. Therefore, co-production of DME can provide a higher CO_2 conversion and a higher selectivity than using MeOH synthesis catalyst only. Also, water is formed by the MeOH dehydration and it can be removed from the process with water gas shift reaction (WGS) and equilibrium composition shifts towards the desired direction [3]. In addition, with the result of thermodynamic analysis, temperature control and heat removal are required because of the exothermic nature of DME synthesis reactions. Consequently, according to thermodynamics point of view, production of DME directly from CO_2 simultaneously is an efficient and promising process for commercial applications. The second reason is that the direct method is more economical than indirect

method. The purification of MeOH synthesis reaction, transportation of MeOH into second reactor, and a separate unit for methanol dehydration reaction to DME are necessary for the indirect method and they are costly. Therefore, the direct method reduces the investment and operational cost.

3.2 Catalysts of Carbon Dioxide Hydrogenation for Dimethyl Ether Synthesis

In recent years, when taking consideration of the fast advancement and the growing accomplishments of DME synthesis, detailed and critical respective research papers have been published regarding the catalytic synthesis of DME [4, 5]. As mentioned earlier in this chapter, gas phase DME could be synthesized in either two-step indirect process or one-step direct process. In both two, process performances such as feed conversion, product distribution or deactivation of the catalyst are strongly affected by catalyst properties. In this part, catalytic system of dimethyl ether production with the effect of both metal and acid catalyst properties on process have been discussed.

3.2.1 Metal Catalyst for Methanol Synthesis from Carbon Dioxide

Catalytic reduction of CO_2 into MeOH is a significant step towards creating a sustainable society and it holds as the main technology for CO_2 utilization system. MeOH can be served as a platform molecule in chemical industries and as an alternative to fossil fuels [6, 7]. Patart et al. [8, 9] reported MeOH synthesis from syngas using solid acid catalysts in 1921 for the first time. On the other hand, BASF [10] introduced the first large scale industrial methanol production using ZnO/Cr_2O_3 catalyst under the conditions of 300-360 °C and 150-250 bars in 1923. However, this catalyst was poisoned by sulfur, chlorine like impurities coming from feed gas easily. After that at the beginning of the 1960s, Imperial Chemical Industries [11] developed a more selective and stable MeOH synthesis catalyst based on copper-zinc oxide and then Johnson Matthey held and licensed this technology. The process was performed at 200-300 °C and 50-100 bar reducing the formation of byproducts using Cu-ZnO-Al_2O_3 catalysts.

In the literature, there are several catalytic systems for the activation of CO_2. Among these studies, copper-based catalysts have been extensively studied with using promoters

because of its improved and better activity [12]. According to the research on heterogeneous catalysts for the hydrogenation of CO_2 the following order of catalytic activity was identified [13];

$$Cu >> Co = Pd = Re > Ni > Fe >> Ru = Pt > Ir = Ag = Rh = Au$$

In general, copper-based catalysts are the most active ones for methanol synthesis from carbon dioxide. However, the catalytic activity depends on metal dispersion, the use of promoter or the choice of support material etc. in any case. Although the main product is carbon monoxide, Cu-ZnO-Al_2O_3 catalyst is still used for industrial purposes [14-16]. In recent years, much effort has been made into understanding of active site of Cu-ZnO-Al_2O_3 [16-20]. However, it is still under debate. Schlögl et al. claim that the synergy between Cu and ZnO resulting from the powerful metal-support interaction has recently been ascribed to CuZn alloy formation where Zn ions were suggested to be the active sites at the step edges of Cu nanoparticles and also Zn coverage was associated quantitatively with the activity [16]. On the other side, recently again the same research group's TEM images suggested that metal-support interaction between Cu-ZnO has resulted in the encapsulation of ZnO over Cu particles on the catalyst which create new active site for MeOH synthesis [17]. The main role of ZnO is that acting as a geometric spacer between Cu particles and resulting in higher number of active sites with Cu metal in ideal dispersion for Cu/ZnO catalyst [21]. Additionally, when Al^{3+} have been added to Cu-ZnO to enhance the stability along with Cu dispersion and metal surface area and this result indicates that CuO-ZnO-Al_2O_3 is an excellent candidate for synthesis of methanol [22]. Also, CO_2 hydrogenation mechanism of CuO-ZnO-Al_2O_3 is that firstly H_2 dissociate at metallic copper, and ZnO site responsible for CO_2 adsorption while Al_2O_3 is using for support and spacer of copper particles. The formation of reactive intermediate on the ZnO has been reported as the rate limiting step [12].

On the basis of the catalyst for MeOH synthesis of Cu/ZnO model, various promoters have been reviewed to improve the CO_2 hydrogenation performance for methanol synthesis. Zhang et al. [23] investigated the promoter effect of SiO_2, TiO_2 on CuO-ZnO-Al_2O_3 catalyst. The findings indicated that the CuO dispersion can be improved by all promoters. SiO_2-TiO_2 promoted catalyst's CO_2 conversion enhanced to 15.8% to 23.3% and selectivity of methanol boosted 40.7% to 41.2% compared to bare CuO-ZnO-Al_2O_3. Apart from the Al_2O_3, Ga_2O_3 has been also investigated as Cu-Zn-Ga_2O_3 for MeOH synthesis catalyst [24]. It is found that the particle size of Ga_2O_3 is crucial for promoting the effect of methanol synthesis. For example,

small Ga_2O_3 particles favored Cu^+ formation which enhanced the catalytic performance. However, C1-C2 hydrocarbons can be catalyzed by Ga_2O_3, so it reduced desired product selectivity [25]. Moreover, Cu-ZnO-ZrO_2 type catalyst has also been extensively studied [26-30]. The major advantage of the catalyst is superior water tolerance. Also, because of the acid character of CO_2, the basic locations are required and ZrO_2 enhanced basicity of the catalyst, so CO_2 conversion increases [31].

Even though, it is accepted that Cu-ZnO exhibits a unique functionality for CO_2 activation, it is also needed for further development of catalyst for other metal oxides for methanol synthesis. For example, catalysts with noble metals as active components are frequently used for MeOH synthesis reaction. Bahruji et al.[32] investigated the Pd/ZnO catalyst. The findings showed that during the reaction PdZn alloy is created and it reduces production of CO by RWGS site reaction. Alternatively in the literature, there are different catalytic systems [33] which used Ag[13, 34], Au[35], Mo[36] as active species for methanol synthesis as well.

Recently, oxygen-deficient materials used as active sites are getting attention for methanol synthesis. Ge et al. [37] studied the defective surface of In_2O_3 (110) with surface oxygen vacancies for MeOH synthesis from CO_2 using DFT calculations. Their interesting findings demonstrated that mechanism for MeOH formation in O_{v4} oxygen defective site on D_4 surface is much more favorable for CO_2 activation than previously reported copper-based catalyst. This O_{v4} oxygen defective site stabilizes intermediates from MeOH formation mechanism and it leads to assist CO_2 activation. Martin et al. [38] proposed In_2O_3/ZrO_2 catalyst which accomplished excellent nearly 100% methanol selectivity and 1000 h stability.

Up to now, tertiary CuO-ZnO-Al_2O_3 is very recognized and optimized technology for CO_2 activation and the MeOH synthesis. Since methanol synthesis over copper-based catalyst is very well known, recently much of the efforts in the research concerning DME synthesis have been devoted to study of the MeOH dehydration catalyst.

3.2.2 Acid Catalysts for Dehydration of Methanol

As mentioned earlier, DME is produced with MeOH dehydration reaction using an acid catalyst. For this purpose, alumina and zeolites have been used in MeOH dehydration

extensively. On the other hand, heteropoly acids can be a good candidate for this reaction as well.

One of the solid acid catalysts which is recognized as the efficient MeOH dehydration catalyst is γ-Al_2O_3 because of its low cost, high surface area, good thermal, and mechanical stability [39]. In addition to these, γ-Al_2O_3 can also provide high DME selectivity even if the reaction takes place at higher temperatures with the help of the presence of less strong Lewis acid sites which do not allow to produce side products such as hydrocarbons. However, there are some drawbacks, such as low hydrothermal activity or strong surface hydrophilic ability. A significant amount of water is produced during the reaction and γ-Al_2O_3, mostly Lewis site, tends to adsorb water strongly, causing deactivation of the catalyst. Therefore, γ-Al_2O_3 could not be a good option for DME production by CO_2 hydrogenation.

In addition to the conventional alumina, the other family of solid acid catalyst for dehydration catalysts for DME synthesis is zeolites. Zeolite catalysts are commonly employed as dehydration catalysts for DME because of their advantages of being regenerable and their stability over a wide range of temperature and high hydrothermal stability [40]. It is generally stated that at a temperature range between 240 - 280 °C, HZSM-5 indicates a much greater activity than γ-Al_2O_3 and on Cu-based catalyst, zeolites have more advantages in thermodynamics point of view than γ-Al_2O_3 does [41]. Also, the HZSM-5 is hydrophobic compared to γ-Al_2O_3 [42, 43]. However, HZSM-5 has strong Brønsted acid sites that it can further convert DME into hydrocarbons as side products, therefore some modifications should be made to improve DME selectivity for HZSM-5 [44].

There are very few studies that are using supported heteropoly acids (HPAs) for the dehydration of MeOH. Because they have high Brønsted acidity and tunable acid properties, they are good candidates for production of DME starting with the MeOH. However, heteropoly acids should be supported on metal oxide carriers to be able to utilize them in catalytic applications efficiently because of their low surface area. Ladera et al. [45, 46] pointed out that TiO_2 supported HPAs can enhanced the availability of methanol molecules to acidic site of the catalyst for MeOH dehydration process. Because of the high Brønsted acidity exhibited, HPAs generally give high catalytic performance than other strong catalysts, such as zeolites-ZSM-5, do particularly at low temperatures. For example, Alharbi et al. [47] showed that HPAs exhibit catalytic performances usually better than other solid catalysts for MeOH dehydration. They compared HPAs with ZSM-5 (Si/Al = 10–120) and findings suggested that heteropoly acids

offer up to one order of magnitude increase in turnover frequency for methanol to DME conversion. They explained this superior performance of HPAs by having higher acid site strength.

3.2.3 Multifunctional Catalyst for Direct Dimethyl Ether Synthesis

For direct DME synthesis, the catalyst must be active for both MeOH synthesis and its dehydration. Over the past few years, direct DME synthesis from syngas or CO_2, combining with MeOH synthesis and dehydration of MeOH in a single step, has been extensively studied. Direct DME synthesis from CO_2 mainly relies on the acidity of the dehydration component which is a solid acid catalyst in the catalyst system. In this system, it is beneficial for catalyst which is being inactive for RWGS side reaction and possible hydrocarbons formation from methanol conversion. For example, if the acidity amount of the catalyst is not enough, methanol in the system could not be dehydrated sufficiently. On the other hand, if acidity is too high, the newly formed DME could be convert into hydrocarbons [48] or even coke formation could be seen as well [44, 49]. In addition to optimizing the acidity of dehydration component, optimizing the composition and reaction conditions of two functional components is a very essential point for preparing an active catalyst system for the direct DME synthesis. Also, a huge amount of water formed during the CO_2 hydrogenation into DME should be considered because it limits both the formation and the dehydration of methanol thermodynamically and it leads to a lower DME yield [43].

In Table 3.1, the catalysts reported for the direct hydrogenation of CO_2 to DME in the literature are summarized.

Table 3.1 Summary of the catalysts reported for the direct hydrogenation of CO_2 to DME.

Catalyst	T (°C)	P (bar)	$H_2/CO_2/N_2$	GHSV ($ml_{CO2}g_{cat}^{-1}h^{-1}$)	X_{CO2} (%)	S_{DME} (%)	STY_{DME} ($g_{DME}kg_{cat}^{-1}h^{-1}$)	Ref.
Cu-Zn-Zr/FER	260	50	9/3/1	2030	26	55.7	600	[50]
Cu-Zn-Zr/FER	280	50	9/3/1	2030	30	62	752	[51]
CuO-Fe_2O_3-ZrO_2/HZSM-5	260	30	5/1	250	28.4	64.5	86	[52]
PdZn/TiO_2/ZSM-5	270	20	3/1/1	720	11	32.3	48	[53]
Cu-ZnO-ZrO_2/HZSM-5	243	30	9/3/1	2076	15	25	147	[54]
CuO-ZnO-ZrO_2/WO_x/Al_2O_3	260	30	9/3/1	3000	18.9	15.3	164	[29]

$CuO-ZnO-Al_2O_3$/HZSM-5	260	30	9/3/1	346	27.3	67.1	120	[55]
$CuO-ZnO-ZrO_2/WO_x/ZrO_2$	260	30	9/3/1	1000	21.5	29	271	[56]
Cu-Zn-Zr/MFI	240	50	9/3/1	2307	24	49.3	513	[28]
Cu-Zn-Ga/FER	260	30	9/3/1	2030	21.1	34.9	282	[57]
Cu-Zn-Al/HZSM-5	260	50	3/1	750	31	65	285	[58]
Cu-Zn-Al/Al_2O_3	260	50	3/1	750	20	82	232	[58]
Cu-Zn-Al-Zr/ZSM-5	260	30	3/1	400	25	23.3	43	[59]
Cu-Zn-Al/ZSM-5+CNTs	260	30	3/1	450	46.2	45.2	177	[60]
$CuO-ZnO-ZrO_2/SO_4^{2-}-ZrO_2$	260	20	9/3/1	3750	17.2	25.6	311	[61]
$CuO-ZnO-Al_2O_3$/HZSM-5	260	42	3/1	381	30.5	72	158	[62]
Cu-Zn-Zr-V/ZSM-5	270	30	3/1	1050	32.3	57.8	370	[63]
Cu-Zn-Zr-Pd/ZSM-5	200	30	3/1	450	18.7	73.6	117	[64]
$CuO-TiO_2-ZrO_2$/HZSM-5	250	30	3/1	375	15.6	47.5	52	[65]
Cu-Zn-Al-La/HZSM-5	250	30	3/1	750	43.8	71.2	441	[66]
Cu/Zn/Al Amorphous Si-Al	266	30	3/1	450	47.1	42.4	170	[67]
Cu-Mo/HZSM-5	240	20	3/1	375	12.4	77.2	68	[68]
$CuO-Fe_2O_3-CeO_2$/HZSM-5	260	30	4/1	375	20.9	63.1	93	[69]
Cu-Fe-Ce/HZSM-5	260	30	4/1	375	18.1	52	67	[70]
Cu-Fe-La/HZSM-5	260	30	4/1	375	17.2	51.3	62	[70]

In the first study for direct conversion of CO_2 into DME, γ-Al_2O_3 was used with Cu-ZnO-Al_2O_3 system in a physical mixture. However, Xu et al. [71] demonstrated that the presence of water produced during the reaction has a significant inhibitory impact on the activity of γ-Al_2O_3 as already mentioned in Section 3.2.2. However, the physical combination of γ-Al_2O_3 as an acid catalyst with Cu-ZnO MeOH synthesis catalyst was used extensively in the literature [58]. H-ZSM-5 zeolite, having both Lewis and Brønsted acid sites and water resistance, offers an improvement in long term stability during the reaction than γ-Al_2O_3 does. Therefore, they are extensively used for direct DME synthesis from CO_2. And Aguayo et al. [72] examined the deactivation character of Cu-ZnO-Al_2O_3/γ-Al_2O_3 and Cu-ZnO-Al_2O_3/ZSM-5 hybrid catalysts. When using HZSM-5, it was investigated that zeolites as a solid acid component were less prone to deactivation by coke compare to alumina. Dubois et al. [73] stated that different combination of MeOH synthesis catalyst and different Si/Al ratio of zeolites and they reported that Si/Al=6 of Y-zeolite and Si/Al=10 of were proved to be efficient to achieve high DME selectivity and high yield of MeOH and DME. Frusteri et al. [28] demonstrated that role of acid sites of multifunctional catalysts of Cu-Zn-Zr with HZSM-5 zeolite with range of Si/Al is 27-127. They investigated that it is possible to tune the performance of catalyst and deactivation properties with playing of acidic character of zeolite.

If catalyst has a high Si/Al ratio, it exhibits a high water resistance; however, it has a low capacity to convert MeOH into DME. On the other hand, catalyst which has a low Si/Al ratio shows a high capacity for the dehydration of methanol, but it has a low DME selectivity with poor resistance in presence of water.

These explanations show it is required that a more detailed understanding of the basic mechanism and relationships between the active species of metallic and acid sites of the multifunctional catalysts.

References

[1] T. Witoon, T. Permsirivanich, N. Kanjanasoontorn, C. Akkaraphataworn, A. Seubsai, K. Faungnawakij, C. Warakulwit, M. Chareonpanich, J. Limtrakul, Direct synthesis of dimethyl ether from CO_2 hydrogenation over Cu-ZnO-$ZrO_2SO_4^{2-}$-ZrO_2 hybrid catalysts: Effects of sulfur-to-zirconia ratios, Catalysis Science and Technology, 5 (2015) 2347-2357.

[2] V. M. Mysov, Application of Polyfunctional Catalysis in Synthesis of Motor Fuels from CO_2 as an Approach to the Problem of CO_2 Utilization, Chemistry for Sustaniable Development, 11 (2003) 197-207.

[3] T. Takeguchi, Effect of the property of solid acid upon syngas-to-dimethylether conversion on the hybrid catalysts composed of Cu–Zn–Gaand solid acids, Applied Catalysis A: General 192 (2000) 201–209.

[4] J. Sun, G. Yang, Y. Yoneyama, N. Tsubaki, Catalysis Chemistry of Dimethyl Ether Synthesis, ACS Catalysis, 4 (2014) 3346-3356.

[5] G. Olah, Chemical Recycling of Carbon Dioxide to Methanol and Dimethyl Ether: From Greenhouse Gas to Renewable, Environmentally Carbon Neutral Fuels and Synthetic Hydrocarbons, Journal of Organic Chemistry, 74 (2009) 487–498.

[6] G.A. Olah, Beyond oil and gas: The methanol economy, Angewandte Chemie International Edition, 44 (2005) 2636-2639.

[7] G.A. Olah, Towards oil independence through renewable methanol chemistry, Angewandte Chemie International Edition, 52 (2013) 104-107.

[8] G. Patart, in French Patent 540, 1921, p. 343.

[9] C. Lormand Industrial Production of Synthetic Methanol, Industrial and Engineering Chemistry, 17 (1925) 430.

[10] BASF, in German Patents 415 686, 441 433, 462 837, 1923.

[11] ICI, in GB Patents 1 010 871 (1961), 1 159 212 (1969), 1 296 212 (1972).

[12] F. Arena, G. Italiano, K. Barbera, S. Bordiga, G. Bonura, L. Spadaro, F. Frusteri, Solid-state interactions, adsorption sites and functionality of Cu-ZnO/ZrO_2 catalysts in the CO_2 hydrogenation to CH_3OH, Applied Catalysis A: General, 350 (2008) 16-23.

[13] S. Sugawa, Methanol synthesis from CO_2 and H_2 over silver catalyst, Energy Convers. 36 (1995) 665-668.

[14] T. Lunkenbein, J. Schumann, M. Behrens, R. Schlogl, M.G. Willinger, Formation of a ZnO overlayer in industrial Cu/ZnO/Al_2 O_3 catalysts induced by strong metal-support interactions, Angewandte Chemie International Edition, 54 (2015) 4544-4548.

[15] S. Kuld, Quantifying the promotion of Cu catalysts by ZnO for methanol synthesis, Science, 352 (2016) 969.

[16] M. Behrens, The Active Site of MethanolSynthesis over Cu/ZnO/Al_2O_3 Industrial Catalysts, Science, 336 (2012) 893.

[17] T. Lunkenbein, F. Girgsdies, T. Kandemir, N. Thomas, M. Behrens, R. Schlogl, E. Frei, Bridging the Time Gap: A Copper/Zinc Oxide/Aluminum Oxide Catalyst for Methanol Synthesis Studied under Industrially Relevant Conditions and Time Scales, Angewandte Chemie International Edition, 55 (2016) 12708-12712.

[18] C. Tisseraud, C. Comminges, S. Pronier, Y. Pouilloux, A. Le Valant, The Cu–ZnO synergy in methanol synthesis Part 3: Impact of the composition of a selective Cu@ZnO x core–shell catalyst on methanol rate explained by experimental studies and a concentric spheres model, Journal of Catalysis, 343 (2016) 106-114.

[19] O. Martin, C. Mondelli, A. Cervellino, D. Ferri, D. Curulla-Ferre, J. Perez-Ramirez, Operando Synchrotron X-ray Powder Diffraction and Modulated-Excitation Infrared Spectroscopy Elucidate the CO_2 Promotion on a Commercial Methanol Synthesis Catalyst, Angewandte Chemie International Edition 55 (2016) 11031-11036.

[20] C. Tisseraud, C. Comminges, T. Belin, H. Ahouari, A. Soualah, Y. Pouilloux, A. Le Valant, The Cu-ZnO synergy in methanol synthesis from CO_2 Part 2: Origin of the methanol and CO selectivities explained by experimental studies and a sphere contact quantification model in randomly packed binary mixtures on Cu-ZnO coprecipitate catalysts, Journal of Catalysis, 330 (2015) 533-544.

[21] A. T. Aguayo, Kinetic Modeling of Dimethyl Ether Synthesis in a Single Step on a CuO−ZnO−Al2O3 -Al2O3 Catalyst, Industrial and Engineering Chemistry, 46 (2007) 5522-5530

[22] C. Baltes, S. Vukojevic, F. Schuth, Correlations between synthesis, precursor, and catalyst structure and activity of a large set of $CuO/ZnO/Al_2O_3$ catalysts for methanol synthesis, Journal of Catalysis, 258 (2008) 334-344.

[23] L. Zhang, Y. Zhang, S. Chen, Effect of promoter SiO_2, TiO_2 or SiO_2-TiO_2 on the performance of CuO-ZnO-Al_2O_3 catalyst for methanol synthesis from CO_2 hydrogenation, Applied Catalysis A: General, 415-416 (2012) 118-123.

[24] J. Toyır, Catalytic performance for CO_2 conversion to methanol of gallium-promoted copper-based catalysts influence of metallic precursors, Applied Catalysis B: Environmental 34 (2001) 255–266

[25] J. Toyır, Highly effective conversion of CO_2 to methanol over supported and promoted copper-based catalysts influence of support and promoter, Applied Catalysis B: Environmental 29 (2001) 207–215

[26] F. Frusteri, M. Cordaro, C. Cannilla, G. Bonura, Multifunctionality of Cu-ZnO-ZrO_2/H-ZSM5 catalysts for the one-step CO_2-to-DME hydrogenation reaction, Applied Catalysis B: Environmental, 162 (2015) 57-65.

[27] G. Bonura, M. Cordaro, L. Spadaro, C. Cannilla, F. Arena, F. Frusteri, Hybrid Cu–ZnO–ZrO_2/H-ZSM5 system for the direct synthesis of DME by CO_2 hydrogenation, Applied Catalysis B: Environmental, 140-141 (2013) 16-24.

[28] F. Frusteri, G. Bonura, C. Cannilla, G. Drago Ferrante, A. Aloise, E. Catizzone, M. Migliori, G. Giordano, Stepwise tuning of metal-oxide and acid sites of CuZnZr-MFI hybrid catalysts for the direct DME synthesis by CO^2 hydrogenation, Applied Catalysis B: Environmental, 176-177 (2015) 522-531.

[29] Y. Suwannapichat, T. Numpilai, N. Chanlek, K. Faungnawakij, M. Chareonpanich, J. Limtrakul, T. Witoon, Direct synthesis of dimethyl ether from CO 2 hydrogenation over novel hybrid catalysts containing a Cu ZnO ZrO_2 catalyst admixed with WO_x /Al_2O_3 catalysts: Effects of pore size of Al_2O_3 support and W loading content, Energy Conversion and Management, 159 (2018) 20-29.

[30] G. Bonura, C. Cannilla, L. Frusteri, A. Mezzapica, F. Frusteri, DME production by CO_2 hydrogenation: Key factors affecting the behaviour of CuZnZr/ferrierite catalysts, Catalysis Today, 281 (2017) 337-344.

[31] P. Gao, F. Li, N. Zhao, F. Xiao, W. Wei, L. Zhong, Y. Sun, Influence of modifier (Mn, La, Ce, Zr and Y) on the performance of Cu/Zn/Al catalysts via hydrotalcite-like precursors for CO2 hydrogenation to methanol, Applied Catalysis A: General, 468 (2013) 442-452.

[32] H. Bahruji, M. Bowker, G. Hutchings, N. Dimitratos, P. Wells, E. Gibson, W. Jones, C. Brookes, D. Morgan, G. Lalev, Pd/ZnO catalysts for direct CO_2 hydrogenation to methanol, Journal of Catalysis, 343 (2016) 133-146.

[33] S. Kattel, P. Liu, J.G. Chen, Tuning Selectivity of CO2 Hydrogenation Reactions at the Metal/Oxide Interface, J Am Chem Soc, 139 (2017) 9739-9754.

[34] R. Köppel, Copper- and Silver–Zirconia Aerogels: Preparation, Structural Properties and Catalytic Behavior in Methanol Synthesis from Carbon Dioxide, Journal of Catalysis 179 (1998) 515–527

[35] H. Sakurai, Synergism in methanol synthesis from carbon dioxide over gold catalysts supported on metal oxides, Catalysis Today, 29 (1996) 361-365

[36] M.S. Duyar, C. Tsai, J.L. Snider, J.A. Singh, A. Gallo, J.S. Yoo, A.J. Medford, F. Abild-Pedersen, F. Studt, J. Kibsgaard, S.F. Bent, J.K. Norskov, T.F. Jaramillo, A Highly Active Molybdenum Phosphide Catalyst for Methanol Synthesis from CO and CO_2, Angewandte Chemie International Edition, 57 (2018) 15045-15050.

[37] J. Ye, C. Liu, D. Mei, Q. Ge, Active oxygen vacancy site for methanol synthesis from CO_2 hydrogenation on In_2O_3(110): A DFT study, ACS Catalysis, 3 (2013) 1296-1306.

[38] O. Martin, A.J. Martin, C. Mondelli, S. Mitchell, T.F. Segawa, R. Hauert, C. Drouilly, D. Curulla-Ferre, J. Perez-Ramirez, Indium Oxide as a Superior Catalyst for Methanol Synthesis by CO_2 Hydrogenation, Angewandte Chemie International Edition, 55 (2016) 6261-6265.

[39] A.R. Keshavarz, M. Rezaei, F. Yaripour, Nanocrystalline gamma-alumina: A highly active catalyst for dimethyl ether synthesis, Powder Technology, 199 (2010) 176-179.

[40] M. Aresta, A. Dibenedetto, E. Quaranta, State of the art and perspectives in catalytic processes for CO_2 conversion into chemicals and fuels: The distinctive contribution of chemical catalysis and biotechnology, Journal of Catalysis, 343 (2016) 2-45.

[41] A. García-Trenco, A. Martínez, Direct synthesis of DME from syngas on hybrid CuZnAl/ZSM-5 catalysts: New insights into the role of zeolite acidity, Applied Catalysis A: General, 411-412 (2012) 170-179.

[42] V. Vishwanathan, K.-W. Jun, J.-W. Kim, H.-S. Roh, Vapour phase dehydration of crude methanol to dimethyl ether over Na-modified H-ZSM-5 catalysts, Applied Catalysis A: General, 276 (2004) 251-255.

[43] Z. Azizi, M. Rezaeimanesh, T. Tohidian, M.R. Rahimpour, Dimethyl ether: A review of technologies and production challenges, Chemical Engineering and Processing: Process Intensification, 82 (2014) 150-172.

[44] D. Mao, W. Yang, J. Xia, B. Zhang, Q. Song, Q. Chen, Highly effective hybrid catalyst for the direct synthesis of dimethyl ether from syngas with magnesium oxide-modified HZSM-5 as a dehydration component, Journal of Catalysis, 230 (2005) 140-149.

[45] R.M. Ladera, J.L.G. Fierro, M. Ojeda, S. Rojas, TiO_2-supported heteropoly acids for low-temperature synthesis of dimethyl ether from methanol, Journal of Catalysis, 312 (2014) 195-203.

[46] R.M. Ladera, M. Ojeda, J.L.G. Fierro, S. Rojas, TiO_2-supported heteropoly acid catalysts for dehydration of methanol to dimethyl ether: relevance of dispersion and support interaction, Catalysis Science & Technology, 5 (2015) 484-491.

[47] W. Alharbi, E.F. Kozhevnikova, I.V. Kozhevnikov, Dehydration of Methanol to Dimethyl Ether over Heteropoly Acid Catalysts: The Relationship between Reaction Rate and Catalyst Acid Strength, ACS Catalysis, 5 (2015) 7186-7193.

[48] M. Stiefel, R. Ahmad, U. Arnold, M. Döring, Direct synthesis of dimethyl ether from carbon-monoxide-rich synthesis gas: Influence of dehydration catalysts and operating conditions, Fuel Processing Technology, 92 (2011) 1466-1474.

[49] D. Jin, Dimethyl ether synthesis via methanol and syngas over rare earth metals modified zeolite Y and dual Cu–Mn–Zn catalysts, Fuel, 86 (2007) 2707-2713

[50] F. Frusteri, M. Migliori, C. Cannilla, L. Frusteri, E. Catizzone, A. Aloise, G. Giordano, G. Bonura, Direct CO_2 -to-DME hydrogenation reaction: New evidences of a superior behaviour of FER-based hybrid systems to obtain high DME yield, Journal of CO_2 Utilization, 18 (2017) 353-361.

[51] G. Bonura, F. Frusteri, C. Cannilla, G. Drago Ferrante, A. Aloise, E. Catizzone, M. Migliori, G. Giordano, Catalytic features of CuZnZr–zeolite hybrid systems for the direct CO_{2s}-to-DME hydrogenation reaction, Catalysis Today, 277 (2016) 48-54.

[52] R.W. Liu, Z.Z. Qin, H.B. Ji, T.M. Su, Synthesis of dimethyl ether from CO_2 and H_2 using a Cu-Fe-Zr/HZSM-5 catalyst system, Industrial and Engineering Chemistry Research, 52 (2013) 16648-16655.

[53] H. Bahruji, R.D. Armstrong, J. Ruiz Esquius, W. Jones, M. Bowker, G.J. Hutchings, Hydrogenation of CO_2 to Dimethyl Ether over Brønsted Acidic PdZn Catalysts, Industrial and Engineering Chemistry Research, 57 (2018) 6821-6829.

[54] G. Bonura, M. Cordaro, C. Cannilla, A. Mezzapica, L. Spadaro, F. Arena, F. Frusteri, Catalytic behaviour of a bifunctional system for the one step synthesis of DME by CO_2 hydrogenation, Catalysis Today, 228 (2014) 51-57.

[55] Y. Hu, Y. Zhang, J. Du, C. Li, K. Wang, L. Liu, X. Yu, K. Wang, N. Liu, The influence of composition on the functionality of hybrid Cu-ZnO-Al_2O_3/HZSM-5 for the synthesis of DME from CO_2 hydrogenation, RSC Advances, 8 (2018) 30387-30395.

[56] T. Witoon, P. Kidkhunthod, M. Chareonpanich, J. Limtrakul, Direct synthesis of dimethyl ether from CO_2 and H_2 over novel bifunctional catalysts containing CuO-ZnO-ZrO_2 catalyst admixed with WO_x /ZrO_2 catalysts, Chemical Engineering Journal, 348 (2018) 713-722.

[57] G. Bonura, C. Cannilla, L. Frusteri, F. Frusteri, The influence of different promoter oxides on the functionality of hybrid CuZn-ferrierite systems for the production of DME from CO_2-H_2 mixtures, Applied Catalysis A: General, 544 (2017) 21-29.

[58] S.P. Naik, T. Ryu, V. Bui, J.D. Miller, N.B. Drinnan, W. Zmierczak, Synthesis of DME from CO_2/H_2 gas mixture, Chemical Engineering Journal, 167 (2011) 362-368.

[59] Y. Zhao, Effects of ZrO_2 on the Performance of CuO-ZnO-Al_2O_3 HZSM-5 Catalyst for Dimethyl Ether Synthesis from CO_2 Hydrogenation, Journal of Natural Gas Chemistry 16 (2007) 389-392.

[60] F. Zha, H. Tian, J. Yan, Y. Chang, Multi-walled carbon nanotubes as catalyst promoter for dimethyl ether synthesis from CO_2 hydrogenation, Applied Surface Science, 285 (2013) 945-951.

[61] C. Temvuttirojn, N. Chuasomboon, T. Numpilai, K. Faungnawakij, M. Chareonpanich, J. Limtrakul, T. Witoon, Development of SO_4^{2-}-ZrO_2 acid catalysts admixed with a CuO-ZnO-ZrO_2 catalyst for CO_2 hydrogenation to dimethyl ether, Fuel, 241 (2019) 695-703.

[62] S. Ren, W.R. Shoemaker, X. Wang, Z. Shang, N. Klinghoffer, S. Li, M. Yu, X. He, T.A. White, X. Liang, Highly active and selective Cu-ZnO based catalyst for methanol and dimethyl ether synthesis via CO_2 hydrogenation, Fuel, 239 (2019) 1125-1133.

[63] Y. Zhang, D. Li, Y. Zhang, Y. Cao, S. Zhang, K. Wang, F. Ding, J. Wu, V-modified CuO-ZnO-ZrO_2/HZSM-5 catalyst for efficient direct synthesis of DME from CO_2 hydrogenation, Catalysis Communications, 55 (2014) 49-52.

[64] K. Sun, W. Lu, M. Wang, X. Xu, Low-temperature synthesis of DME from CO_2/H_2 over Pd-modified CuO-ZnO-Al_2O_3-ZrO_2/HZSM-5 catalysts, Catalysis Communications, 5 (2004) 367-370.

[65] S. Wang, D. Mao, X. Guo, G. Wu, G. Lu, Dimethyl ether synthesis via CO_2 hydrogenation over CuO-TiO_2-ZrO_2/HZSM-5 bifunctional catalysts, Catalysis Communications, 10 (2009) 1367-1370.

[66] Dimethyl ether synthesis from CO_2 hydrogenation on La-modified CuO-ZnO-Al_2O_3/HZSM-5 bifunctional catalysts, Journal of Rare Earths, 31 (2013) 470.

[67] F. Zha, J. Ding, Y. Chang, J. Ding, J. Wang, J. Ma, Cu–Zn–Al Oxide Cores Packed by Metal-Doped Amorphous Silica–Alumina Membrane for Catalyzing the Hydrogenation of Carbon Dioxide to Dimethyl Ether, Industrial & Engineering Chemistry Research, 51 (2011) 345-352.

[68] G. X. Qi, DME synthesis from carbon dioxide and hydrogen Cu–Mo/HZSM-5, Catalysis Letters 72 (2001) 121.

[69] X. Zhou, T. Su, Y. Jiang, Z. Qin, H. Ji, Z. Guo, CuO-Fe_2O_3-CeO_2/HZSM-5 bifunctional catalyst hydrogenated CO_2 for enhanced dimethyl ether synthesis, Chemical Engineering Science, 153 (2016) 10-20.

[70] Z.Z. Qin, X.H. Zhou, T.M. Su, Y.X. Jiang, H.B. Ji, Hydrogenation of CO_2 to dimethyl ether on La-, Ce-modified Cu-Fe/HZSM-5 catalysts, Catalysis Communications, 75 (2016) 78-82.

[71] M. Xu, Synthesis of dimethyl ether (DME) from methanol over solid-acid catalysts, Applied Catalysis A: General 149 (1997) 289-301.

[72] A.T. Aguayo, J. Ereña, I. Sierra, M. Olazar, J. Bilbao, Deactivation and regeneration of hybrid catalysts in the single-step synthesis of dimethyl ether from syngas and CO_s, Catalysis Today, 106 (2005) 265-270.

[73] J. L. Dubois, Conversion of CO_2 to Dimethylether and Methanol over Hybrid Catalysts, Chemistry Letters (1992) 1155-1188.

Chapter 4

MATERIALS AND METHODS

4.1 Materials

The commercial methanol synthesis catalyst (MSC), $CuO\text{-}ZnO\text{-}Al_2O_3$ (Alfa Aesar product no. 45776) was studied in this thesis. Tungstophosphoric acid (TPA - $H_3PW_{12}O_{40}$) and mesoporous silica (MCM-41, reagent grade, ~1000 m^2/g) were purchased from Sigma Aldrich. H_2 (99.999 % - Air Liquid) and CO_2 (9.99 % - Linde) were used as reactant.

4.2 Catalyst Preparation

Methanol synthesis catalyst was prepared after crushing and sieving into grain size of 75 mesh.

A set of TPA/MCM-41 solid acid catalysts (SAC), with a TPA:MCM-41 weight ratio of 30:70, 40:60, 60:40, 80:20 (wt:wt), was prepared by impregnation as before [1]. In short, TPA was dried at 90 °C under vacuum for 3 h and then impregnated on MCM-41, which was freshly calcined at 520 °C for 5 h in air. TPA was dissolved in water and mixed on a magnetic stirrer at 100 rpm at room temperature for 15 min. Following the mixing period, freshly calcined MCM-41 was added into the solution. The solution was then mixed for 24 h and dried at 110 °C for 5 h. The dried powder was calcined in air at 250 °C for 4 h.

To prepare the physical mixture of catalysts, the commercial 75 mesh-sized MSC and as-prepared SAC (< 75 mesh) with various TPA loadings were mixed together by simple shaking-mixing in a vessel. The obtained physical mixture of MSC and SAC was denoted as MSC:SAC (*x*:*y*), where *x*:*y* defines the mixing ratio as the ratio of the amount of methanol synthesis catalyst to that of the TPA/MCM-41. The ratios considered in this study are 2:1, 3:1, and 4:1 (wt:wt), while the total amount of the physical mixture was set to 0.2 g.

4.3 Catalyst Characterization Methods

4.3.1 X-Ray Diffraction

X-ray diffraction (XRD) is a common technique for the qualitative study of crystal structures and atomic spacing of a compound. X-ray diffraction is based on constructive interference of monochromatic X-rays and a crystalline sample. These X-rays are generated by a cathode ray tube, filtered to produce monochromatic radiation, collimated to concentrate, and directed toward the sample. The interaction of the incident rays with the sample produces constructive interference when conditions satisfy Bragg's law: $n\lambda = 2d\sin\theta$ where n is an integer, λ is the wavelength of the X-rays, d is the interplanar spacing generating the diffraction, and θ is the diffraction angle. This law relates the wavelength of electromagnetic radiation to the diffraction angle and the lattice spacing in a crystalline sample. These diffracted X-rays are then detected, processed, and counted. By scanning the sample through a range of 2u angles, all possible diffraction directions of the lattice should be attained due to the random orientation of the powdered material. Conversion of the diffraction peaks to d-spacings allows identification of the compound because each compound has a set of unique d-spacings. Typically, this is achieved by comparison of d-spacings with standard reference patterns [2].

In this study, A Bruker D8 Discover X-Ray Diffraction instrument was used with a Cu Kα1 radiation source with an employed wavelength of 1.5418 Å for XRD analysis. Power rating values of the instrument were 40 kV and 40 mA. To detect the diffracted X-rays, a 1D detector (Vantec-1) was used and the divergence slit was set to 1 mm. A 2Θ range between 10-90° with a step size of 0.01263° was used. The samples were prepared by placing approximately 10 mg of catalyst on a double-sided tape, which was attached to a glass slide. Then, the glass side was loaded on to the sample holder. For phase definition, ICDD PDF-4 2018 database was used by subtracting the background.

4.3.2 Ammonia-Temperature Programmed Desorption Measurements (NH_3-TPD)

Temperature programmed desorption (TPD) is a common technique to determine the impact of adsorbed material conduct on the kinetic and thermodynamic parameters of surface desorption process or decomposition reaction. It is very powerful tool for evaluation of active

sites and understanding of the mechanism of catalytic reaction which consist of adsorption, surface reaction and desorption. In theory, the catalyst sample is degassed firstly, then gas molecule like ammonia is adsorbed on catalyst sample, after that sample is heated with using specific temperature program in a stream of inert gas. Some of the reaction products desorb from surface while increasing with temperature and the amount of base desorbed is detected by gas chromatography or mass spectrometry [3, 4]. NH_3-TPD is a commonly used method for quantitatively determining the number of acid sites and acidic strength of catalysis.

In this study, A Micrometrics AutoChem II 2920 instrument equipped with a thermal conductivity detector and an MKS Cirrus 2 mass spectrometer was used to perform NH_3-TPD measurements. Approximately 0.1 g of catalysts were loaded into a U-shaped quartz microreactor for each measurement. Catalysts were pretreated at 250 °C for 2 h under helium flow (50 cm^3 min^{-1}). Then, they were treated in flowing pure NH_3 (50 cm^3 min^{-1}) at 40 °C for 1 h. The physisorbed NH_3 was removed under helium flow for 1 h at 100 °C. Samples were heated up to 700 °C with a ramp rate of 3 °C min^{-1}, while the exit gas stream was monitored by a thermal conductivity detector (TCD). Using the Origin Lab software, the features in the spectrum of NH_3-TPD was then deconvoluted into individual components and the calculated areas under each curve were used to quantify the acid site amount using the pre-calibrated signals collected by the TCD.

The active sites for dehydration of MeOH to DME are acid sites which is a very significant feature for the multifunctional catalysts working in direct DME synthesis reaction. For solid acid catalyst, it is essential to choose the base probe sample to obtain TPD measurements and typically a small base molecule like ammonia which has strong basicity, ability to absorb selectively on sites of different acid strengths and to detect of acidic sited even located into very narrow pores [5].

4.3.3 Fourier Transform Infrared (FTIR) Spectroscopy

Fourier transform infrared (FTIR) is a non-destructive spectroscopy technique to identify the functional groups of the sample via an infrared light sources to measure absorption. The fundamental theory is that light at different frequencies is absorbed by the bonds between different elements. FTIR offers specific information for vibration and rotation of bonding and molecular structures of the chemical and it represents a fingerprint of sample. Therefore,

molecular species can be determined qualitatively. Also, it is possible determine amount of material present via amount of the peak in the spectrum quantitatively. Molecules are continuously vibrating with stretching or bending modes in order to absorb IR radiation. IR radiation has enough energy to vibrate them and IR radiation can be absorbed only at certain wavelengths. Chemical bonds vibrate at unique frequencies, absorbing radiation at wavelengths that match their vibration modes when subjected to infrared radiation. Measuring the absorption of radiation as a function of frequency creates raw data then Fourier transform which is a mathematical process convert raw data into readable spectrum. This spectrum can be used to identify functional groups.

FTIR measurements were collected using a Bruker Vertex 80v FTIR spectrometer equipped with a vacuum chamber in transmission mode. The samples were packed between two KBr windows in a sample holder. For each measurement, an average of 256 scans were averaged where resolution was set to 4 cm^{-1} under vacuum. Before each measurement, 128 background scans were collected.

4.3.4 Brunauer-Emmet-Teller (BET), Barrett-Joyner-Halenda (BJH) Analyses

The theory of BET relies on the physical adsorption of gas molecules such as nitrogen on a solid surface to evaluate the material's specific surface area. The quantity of absorbed gas on the surface is calculated according to a monolayer. Tests are performed at liquid nitrogen temperature and the theory of BET is used for calculations.

In this study, Brunauer-Emmet-Teller (BET) and Barrett-Joyner-Halenda (BJH) analyses were done by using a Micrometrics ASAP 2020 physisorption analyzer For each experiment 100 mg samples were degassed at 250 °C for 4 h. N_2 adsorption was applied at -196 °C using *t*-method between 0.091 and 0.4 P/P_0 to determine surface areas.

4.4 Catalytic Performance and Product Analysis by Micro-Gas Chromatography

Catalytic performance tests for CO_2 hydrogenation were carried out in homemade high-pressure flow reactor system which is showed in Fig. 4. The design and construction of the system is one of the main aim of this study. The reactant gas mixture set by Bronkhorst (model no: F-201CV-1K0) mass flow controllers (MFCs). The temperature of the reactor was measured

in the middle of the fixed-bed with a movable thermocouple. After reactor outlet, all tubings were heated to avoid condensation of the water formed in the reaction. Catalytic performance tests were carried out in a once-through ½"-stainless-steel fixed-bed flow reactor, loaded with 0.2 g of physical mixing catalysts, diluted with inert same-sized α-Al_2O_3 (0.8 g) (Sigma Aldrich A1522), which was calcined at 1200 °C for 5 h prior to use. Quartz wool was used to fix the sample in the reactor. Blank experiments confirmed that there was no activity of the reactor filled with glass beads and quartz wool at the reaction conditions considered. The reactor was located in a 3-zone furnace (Thermcraft,model no: XST-3-0-12-3C2-E26-X) with three independent temperature controllers, operating at a total pressure of 45 bar and a temperature range from 220 to 250 °C at a gas hourly space velocity (GHSV) ranging between 7000 and 40 000 mL CO_2 g_{cat}^{-1} h^{-1} and a gas mixture containing a gas mixture of H_2:CO_2 with a molar ratio of 3:1. Prior to each experiment, the catalyst was reduced *in situ* in flowing H_2 (100 mL min^{-1}) for 2 h at 5 bar and 250 °C. The CO_2 conversion and yields of products over the physical mixing catalysts reached a pseudo-steady state after 2 h.

The product stream was analyzed by online Agilent 490 Micro Gas Chromatography (Micro GC) System equipped with four independent analytical channels. Micro GC is very compact and miniaturized instrument. Each channel has own micro-machined injector, electronic carrier gas control, narrow-bore analytical column and micro thermal conductivity detector. The first channel consists of two series 5 m PBQ and 10 m Molecular Sieve 5A PLOT with inner diameter of 0.25 mm ID molecular sieve column for detection of H_2, CO, CH_4; second channel has PoraPLOT U (0.25 mm ID, 10 m) for detection of CO_2, C2-C3 hydrocarbons and oxygenated molecules like methanol and DME; third channel has Alumina KCl PLOT (0.25 mm ID, 10 m), for detection of C2-C6 hydrocarbons; and forth column has 8m CP-Sil 5 CB (0,15 mm ID) columns for detection of C6-C12 hydrocarbons. All channel has back flush option to protect column against from carbon dioxide and moisture. High purity argon (99.999%) for Molecular Sieve 5A PLOT column and helium (99.999 %) for PoraPLOT U, Alumina KCl PLOT and CP-Sil 5 CB columns were using as carrier gases.

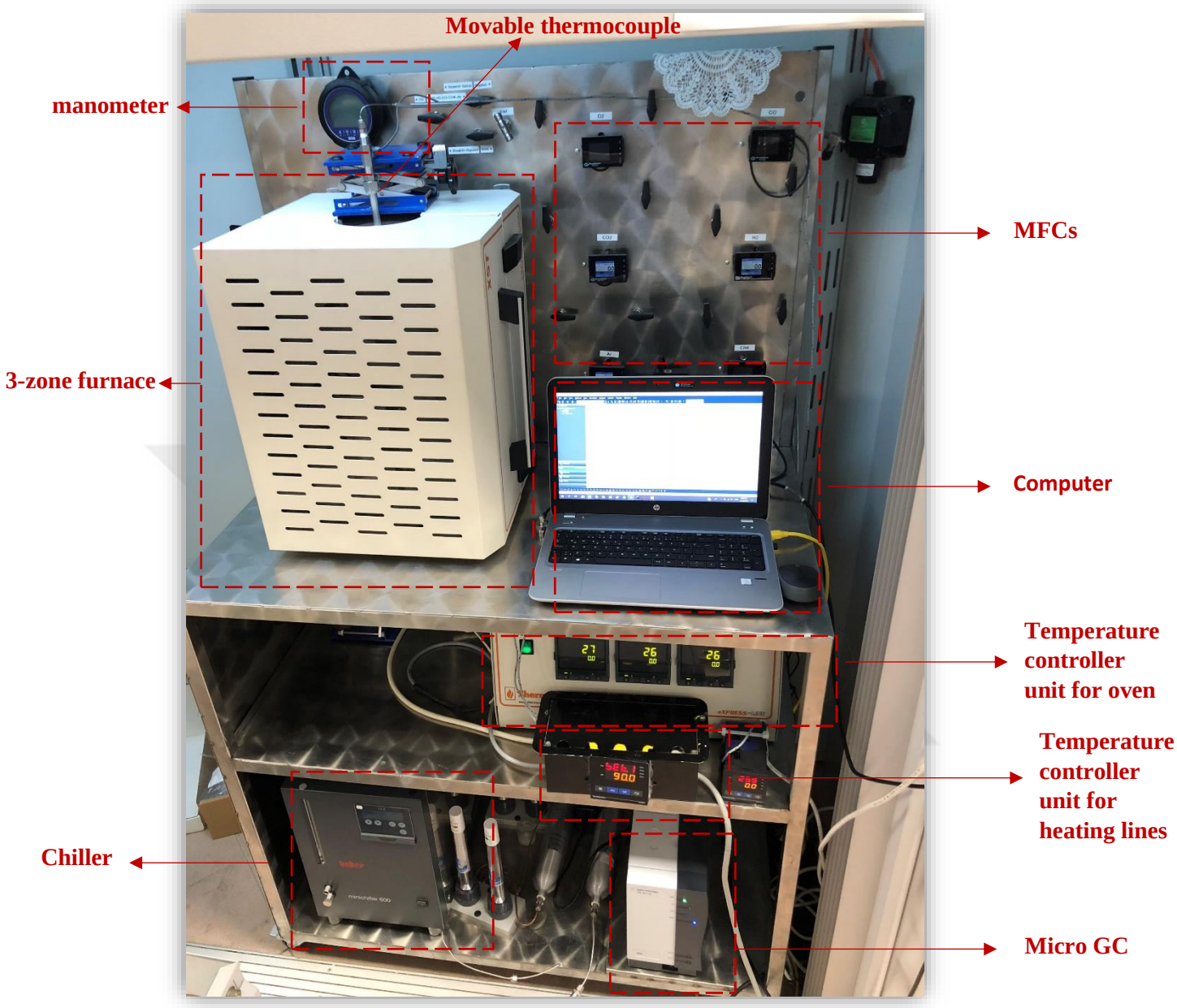

Fig. 4.1 Homemade high-pressure flow reactor system for CO_2 hydrogenation reaction.

The reactor system which is shown in Fig.4.1 has six independent MFCs (Bronkhorst; F-201CV-1K0) with a range of 0-500 mL min^{-1} for CO_2, H_2, Ar, CH_4, CO, O_2 gases. All MFCs are calibrated using 10 mL-glass bubble meters. CO_2, H_2 and Ar gases are connected to system, after gas regulator all gas lines connected to 15-micron line-type filters and check-valves in order not to back flow.

Fig. 4.2 (A) Pneumatic valve for H_2; (B) CO and H_2 detectors; (C) Control Panel of alarm.

Hydrogen cylinder's regulator also connected to pneumatic valve which is shown in Fig. 4.2 (A). Also, CO and CH_4 have pneumatic valve as well. During the reaction, if an unexpected hydrogen leakage occurs or the production of a high amount of CO, the detectors which shown in Fig. 4.2 (B) detect these gases and the audio and visual alarm from the control panel in Fig. 4.2 (C) directly interrupts the gas flow through the pneumatic valves. Leak test of the system was done up to 70 bar with overnight by using 5% H_2:N_2 mixture. During the leak tests, leak was detected via Dräeger brand mobile gas detector, which was calibrated to CO_2, H_2, Ar, CH_4, CO, O_2.

Inside pressure of the reactor were measured by WIKA-wireless (0-100 bar) brand digital manometer. Reactor pressure was regulated with an Equilibar (model no: BPR; EPR 3000) back-pressure regulator. After the BPR, we have two options either we can collect products as liquid using condenser which is shown in Fig. 4.3 and chiller (HUBER-Minichiller 600 OLÉ) or as gas sample by heating all lines. In this study, we collected gas product.

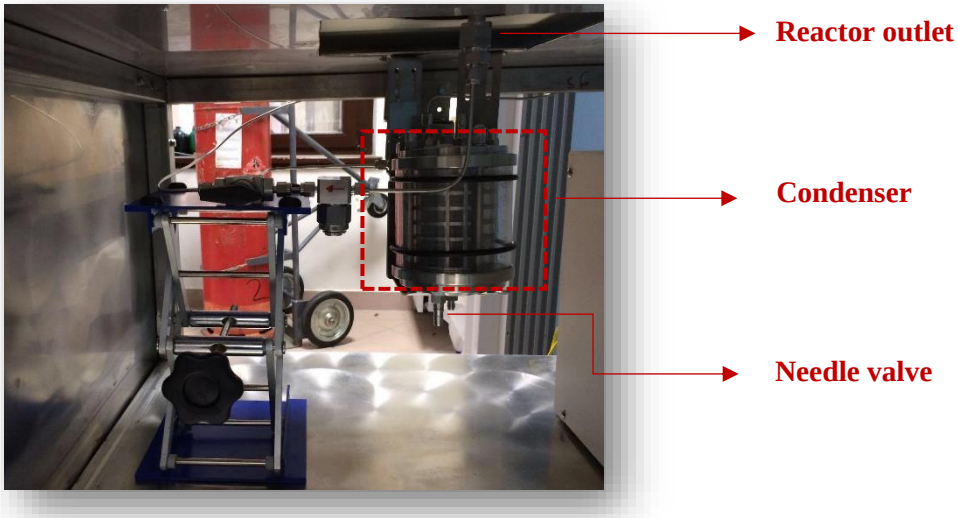

Fig. 4.3 Condenser which connected to chiller to collect liquid products in the reactor system.

Reaction products and unconverted CO_2 and H_2 were analyzed by the Micro GC as mentioned above. Products detection limits of the Micro GC were summarized in Table 4.1. For analysis, we calibrated all gas sample and MeOH. Calibrations for each gas was done by mole-based amounts corresponding to area percent on the Micro GC chromatogram. The methods which was used in calibration was summarized in Table 4.2 The Simply, all gas (CO_2, H_2, CO, and DME) samples were sent to the reactor at different flow rates set by the mass flow controllers. Only MeOH was calibrated by using a Tedlar-bag®. For this purpose, a known amount of liquid MeOH was injected into a Tedlar-bag filled with argon. And then heated MeOH vapor was sent directly to the inlet of Micro GC. Corresponding areas were obtained from the Micro GC, then calibration lines were created. Calibration equation constants are given in Table 4.3.

Table 4.1 Detection limits of gas components with the Micro GC.

Gas Components	Mix. Detection Limit (ppm)	Max. Detection Limit (vol.%)	Channel and Column for Analysis
CO_2	5	100	Channel 2: PoraPLOT U
CO	30	100	Channel 1: Molecular Sieve 5A PLOT
H_2	5	100	Channel 1: Molecular Sieve 5A PLOT
CH_4	30	100	Channel 1: Molecular Sieve 5A PLOT
Ar	30	100	Channel 1: Molecular Sieve 5A PLOT
N_2	30	100	Channel 1: Molecular Sieve 5A PLOT
O_2	30	100	Channel 1: Molecular Sieve 5A PLOT
MeOH (CH_3OH)	5	100	Channel 2: PoraPLOT Q
DME (CH_3OCH_3)	5	100	Channel 2: PoraPLOT Q
Light Olefins (C2-C3)	5	100	Channel 2: PoraPLOT Q
C2-C6 Hydrocarbons	5	100	Channel 3: Alumina KCl PLOT
C6-C12 Hydrocarbons	5	100	Channel 4: CP-Sil 5 CB
Formaldehyde(CH_2O)	100	100	Channel 2: PoraPLOT Q
H_2O	500	1	Channel 2: PoraPLOT Q

Table 4.2 Agilent 490 Micro GC calibration method properties of columns.

Description	**Channel 1**	**Channel 2**	**Channel 3**	**Channel 4**
Carrier Gas	Argon	Helium	Helium	Helium
Description	5m PBQ + 10m MS5A Heated, BF, UM	10m PPQ Heated Injector, Backflush	10m Al_2O_3/KCl Heated Injector Backflush	8m 5CB Heated Injector
Injector Temperature (°C)	110	110	110	110
Injection Time (ms)	40	10	10	70
Backflush Time (s)	60	10	30	-
Column Temperature (°C)	80	100	100	130
Pressure Mode	Static	Static	Static	Static
Initial Pressure (kPa)	150	205	70	205
Detector State	ON	ON	ON	ON
TCD temp limit check	ON	ON	ON	ON
Invert Signal	ON	OFF	OFF	OFF
Sensitivity	Auto	Auto	Auto	Auto
Sampling Frequency (Hz)	100	100	100	100
Run Time (s)	600	600	600	600
Acquisition Delay (s)	0	0	0	0
Stabilizing Time (s)	5	5	5	5
Sample Time (s)	30	30	30	30
Sample Line Temperature (°C)	110	110	110	110
Continuous Flow	OFF	OFF	OFF	OFF
Flush Cycle	1 cycle	1 cycle	1 cycle	1 cycle

Table 4.3 Calibration equation constants for the gas compounds using Micro GC method which is summarized in Table 4.2. (*y=mx+n; x=area under the GC chromatogram peak, y=moles of component*).

Components	**Calibration Equations**	**m**	**n**	R^2
CO_2	$y = 8{,}6009037*10^{-6}\ x - 2{,}7957281*10^{0}$	$8{,}6009037*10^{-6}$	$-2{,}7957281$	$9{,}9948388*10^{-1}$
H_2	$y = 5{,}0550715*10^{-7}\ x + 3{,}7852410*10^{-1}$	$5{,}0550715*10^{-7}$	$3{,}7852410*10^{-1}$	$9{,}9937602*10^{-1}$
CO	$y = 7{,}1854997*10^{-6}\ x + 2{,}1546737*10^{-1}$	$7{,}1854997*10^{-6}$	$2{,}1546737*10^{-1}$	$9{,}9770292*10^{-1}$
MeOH	$y = 7{,}4266616*10^{-6}\ x + 3{,}3245744*10^{-2}$	$7{,}4266616*10^{-6}$	$3{,}3245744*10^{-2}$	$9{,}9918434*10^{-1}$
DME	$y = 5{,}7569209*10^{-6}\ x + 8{,}5484259*10^{-3}$	$5{,}7569209*10^{-6}$	$8{,}5484259*10^{-3}$	$9{,}9955320*10^{-1}$

References

[1] E. Kocaman, Ö. Akarçay, N. Bağlar, S. Çelebi, A. Uzun, Isobutene oligomerization on MCM-41-supported tungstophosphoric acid, Molecular Catalysis, 457 (2018) 41-50.

[2] A.A. Bunaciu, E.G. Udristioiu, H.Y. Aboul-Enein, X-ray diffraction: instrumentation and applications, Crit Rev Anal Chem, 45 (2015) 289-299.

[3] T. Ishii, T. Kyotani, Temperature Programmed Desorption, (2016) 287-305.

[4] S. L.M. Schroeder,Temperature-Programmed Desorption, Advanced Physical Chemistry (2002).

[5] F. Arena, A characterization study of the surface acidity of solid catalysts by temperature programmed methods, Applied Catalysis A: General 170 (1998) 127-137

Chapter 5

CONVERSION OF CO_2 INTO DIMETHYL ETHER ON A PHYSICAL MIXTURE OF TPA/MCM-41 AND CuO-ZnO-Al_2O_3[1]

5.1 Introduction

Carbon dioxide (CO_2) plays an important role in the natural carbon cycle [1]. However, the increase in CO_2 emissions causes global warming and climate changes because of the so-called 'greenhouse effect'. Therefore, the chemical recycling of CO_2 to alternative fuels offers a prospective solution for these environmental concerns and provides new opportunities for sustainable future [2-4]. In this view, conversion of CO_2 into liquid fuels is a promising approach [5]. Much effort is now being put on CO_2 conversion to methanol (MeOH) [6, 7], because MeOH can be directly utilized in fuel cells or can be served as a platform molecule in many different chemical industries [8, 9].

Very recently, there appeared several promising reports of utilizing these methanol synthesis catalysts in different physical mixtures with catalyst possessing acid function to synthesize various products catalysts [10-12]. In these studies, the MeOH produced on the methanol synthesis catalyst is used as a platform molecule and converted into valuable products on the acid catalyst via well-known mechanisms such as methanol-to-hydrocarbons, methanol-to-olefins, and methanol-to-aromatics [13-16]. Among these examples, physically mixing an In_2O_3-based catalyst having a superior selectivity to methanol (~100%) from CO_2 hydrogenation [17] with HZSM-5, Gao et al. [15] demonstrated that C_5–C_{11} hydrocarbons can be produced with a considerably very high selectivity of 78.6% under 340 °C and 30 bar. In the proposed reaction pathway, CO_2 first was converted to methanol on the In_2O_3 surface, which was further transformed into higher chain hydrocarbons on HZSM-5. In a different study, a methanol synthesis catalyst,

[1] The contents of this chapter have been prepared for publication in a scientific journal. The manuscript including this information presented in the chapter will soon be submitted to a catalysis journal. It has been reformatted to meet the requirements of this thesis.

ZnZrO, was mixed with SAPO-34 to obtain an exceptionally high selectivity to lower olefins of in the range of 80-90% at 380 °C and 20 bar [13]. Moreover, Ni et al. [16] illustrated that a physical mixture of $ZnAlO_x$ with HZSM-5 provided 73.9% selectivity for aromatics with trace amount of CH_4 formation under 320 C and 30 bar.

In this study, we aimed at contributing these efforts focusing specifically on the production of dimethyl ether (DME) as the final product. We focused on DME because it can be used as an intermediate to produce several value-added products (gasoline, aromatics, and olefins) or as an alternative fuel [18-20]. And it is the simplest ether without any C–C bonds; it is a colorless, nontoxic, and environmentally friendly [21]. Because of its similar physical and chemical properties, it has a potential of substituting liquid petroleum gas (LPG) [22]. Besides, it is considered as a prospective future synthetic fuel owing to its high cetane number, more complete combustion, and low emission of toxic gases, such as SO_x, NO_x [23].

In the literature, the synthesis of DME from synthesis gas (a mixture of CO and H_2 with trace amount of CO_2) is a common process [24-28]. Conventionally, there are two main paths: a two-step and a direct process. In a two-step process, first MeOH is synthesized over a metallic catalyst, and then DME is produced on an acid catalyst by the dehydration of MeOH in a subsequent second reactor. In the direct one-step process, on the other hand, a multifunctional catalyst combining a metallic function with acid function is used in a single-pass reactor [19]. In the recent years, the single-pass process is becoming very attractive as it offers opportunities for improving the conversion by continuously removing methanol from the system, thereby reducing the thermodynamic limitations.

In the studies focusing on the CO_2 hydrogenation, the dehydration of MeOH into DME is conducted mostly over γ-alumina or zeolites. Among these two solid acid catalysts, the catalytic performance and the lifetime of γ-Al_2O_3 are greatly limited by its low activity and hydrothermal stability [29]. As in the case of production of other hydrocarbons from CO_2, extensive studies have been undertaken to use zeolites as an acid catalyst for the DME synthesis in the literature. Among the zeolites, H-ZSM-5 is the most widely studied one [25, 30-46], because of its high performance. However, it also offers a considerable amount of side products, such as hydrocarbons, and even coke are easily produced during DME synthesis [26–28]. As a result, the catalytic activity of H-ZSM-5 rapidly decreases owing to the formation of coke or to deactivation by the presence of water [9,27]. Therefore, there is a strong need for investigating

the potential of different solid acids providing the acid function in the physical mixture for the DME production from CO_2 hydrogenation.

For this purpose, our aim here is to assess the potential of heteropoly acids (HPAs), particularly Keggin-type-heteropoly acids, as the acid function of the physical mixture for the direct conversion of CO_2 into DME. We chose HPAs because of their inherent characteristics, such as high Brønsted acidity, excellent redox stability, and environmentally friendly properties [47]. And more importantly, they were shown to offer up to one order of magnitude increase in the turnover frequency for the dehydration of MeOH into DME compared to that of HZSM-5 [48]. For this purpose, we chose the tungstophosphoric acid (TPA) as the HPA, as it offers the highest acid strength among the commercially available HPAs [49]. However, the TPA has a very low surface area; thus, it needs to be dispersed over high surface area supports. We recently demonstrated that MCM-41, a high surface area mesoporous silica, with a surface area in the order of 1000 $m^2\ g^{-1}$, is an excellent platform for the dispersion of TPA at exceptionally high TPA loadings [49]. Our data on isobutene oligomerization showed that catalytic properties of the TPA can be tuned by the choice of TPA loading on MCM-41. Based on these previous results, we posit that such a family of TPA/MCM-41 (SAC) catalyst can offer a high potential for assessing the performance of HPAs as an acid function to convert CO_2 into DME in a single-pass.

For this purpose, we used an ordinary commercial catalyst, CuO-ZnO-Al_2O_3, as the methanol synthesis catalyst (MSC) component of the physical mixture. Even though this commercial catalyst was mainly optimized for the synthesis of methanol from the synthesis gas, we chose it here as the MeOH synthesis catalyst from CO_2 hydrogenation, because its catalytic properties are well-documented for this reaction as well [50, 51].

We systematically investigated different mixing ratios, TPA loadings, and reaction conditions to optimize the DME production rate from CO_2 hydrogenation. Results illustrated that a physical mixture of MSC:SAC prepared at a mixing ratio of 4:1 (wt:wt) including 60 wt% TPA-loaded SAC provided a DME production rate of 1551.5 $g_{DME}\ kg_{cat}^{-1}\ h^{-1}$, to the best of our knowledge, more than twice of the highest value ever reported in the literature on the direct conversion of CO_2 into DME. Considering that this high DME production rate was obtained in a physical mixture containing a commercial MeOH synthesis catalyst, optimized specifically for synthesis gas, our results present a broad potential of TPA/MCM-41 solid acid

catalysts, especially when used together with a methanol synthesis catalyst specifically designed for high performance in CO_2 hydrogenation.

5.2 Results and Discussion

5.2.1 Characterization of TPA/MCM-41 Catalysts

Table 5.1 shows the morphological properties of the SACs prepared at different TPA loadings. As shown in Table 5.1, results from the BET and BJH analyses revealed that the surface area and pore volume decreased from 520 m^2/g and 0.45 cm^3/g to 90 m^2/g and 0.05 cm^3/g, respectively, with an increase in TPA loading from 30 to 80 wt%. These decreases in surface area and pore volume of the SACs with increasing TPA loading indicates that the TPA clusters were located inside the MCM-41, consistent with our previous findings [49].

Table 5.1 Results of BET and BJH analyses of the as-prepared TPA/MCM-41 catalysts [49].

TPA Loading (%)	Surface area (m^2/g)	Pore volume (cm^3/g)
30	520	0.45
40	490	0.37
60	280	0.19
80	90	0.05

Fig. 5.1 compares the XRD patterns of SACs prepared at different TPA loadings from 2Θ = 10 to 90°. Accordingly, the bulk TPA has very sharp and distinct characteristic peaks at 24, 35, 38, 53, and 60°, consistent with previous reports characterizing this HPA [52]. However, these features were not detectable in the data of SAC (30:70, wt:wt), indicating that the TPA clusters were highly dispersed at 30 wt% with strong distortions present in their structure, as reported before [49]. Data further indicated that the TPA features started to appear when the TPA loading increased beyond 40 wt%. However, intensity of these features showed slight variations confirming the presence of interaction between TPA and MCM-41 because of

possible changes in electronic environment or orientations of the planes. Based on these results, we infer that there might be some interactions between the TPA clusters and MCM-41. These interactions were investigated in more detail by FTIR spectroscopy.

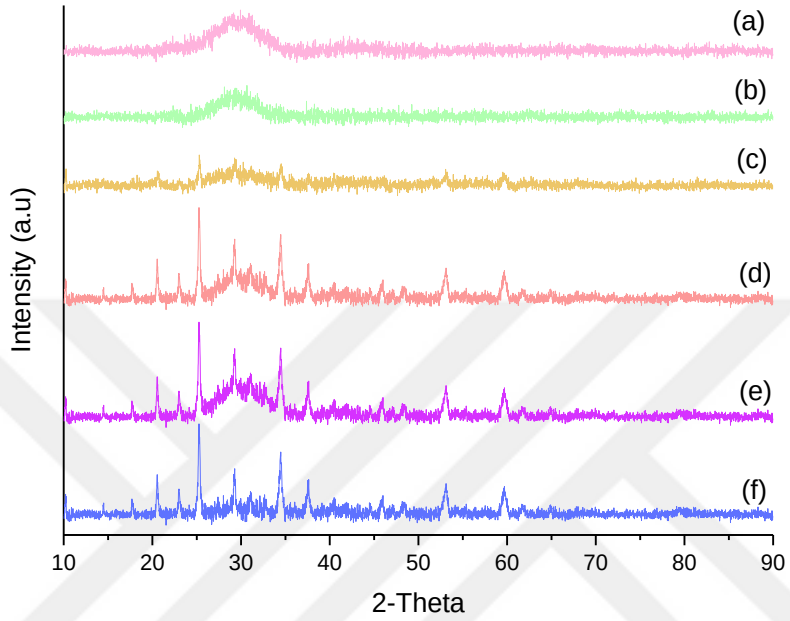

Fig. 5.1 XRD patterns of (a) pristine MCM-41; (b) 30 wt% TPA loaded SAC; (c) 40 wt%-TPA loaded SAC; (d) 60 wt%-TPA loaded SAC; (e) 80 wt%-TPA loaded SAC; (f) bulk TPA.

Fig. 5.2 illustrates the FTIR spectra of MCM-41, TPA, and supported SAC catalysts prepared at different TPA loadings. Four characteristic bands of TPA were observed at 1076 cm^{-1} (asymmetric vibrations of P–O of tetrahedral PO_4), 965 cm^{-1} (stretching modes of the terminal W=O), 881 cm^{-1} (octahedral corner-sharing W–O_b–W), and 770 cm^{-1} (octahedral edge-sharing W–O_c–W). The presence of these characteristic bands on the spectra of SACs with a TPA loading of 40, 60, and 80 wt% indicate the presence of TPA species on the support [53]. However, the IR features of TPA clusters were not detectable in SAC with a TPA loading of 30 wt%, indicating a strong distortion of the TPA cluster, as reported previously by Kocaman et al.[49], Zhang et al.[54], and Berry et al.[55]. These groups independently reported the presence of significant differences in the FTIR spectra of the supported HPAs compared to their bulk counterparts. Accordingly, the characteristic bands were shifted and appeared weaker in intensity. In particular, the band at 805 cm^{-1} characterizing the vibration of W−O_c−W was

shifted linearly to higher wavenumbers, indicating the presence of strong interactions between the TPA clusters and the support [49].

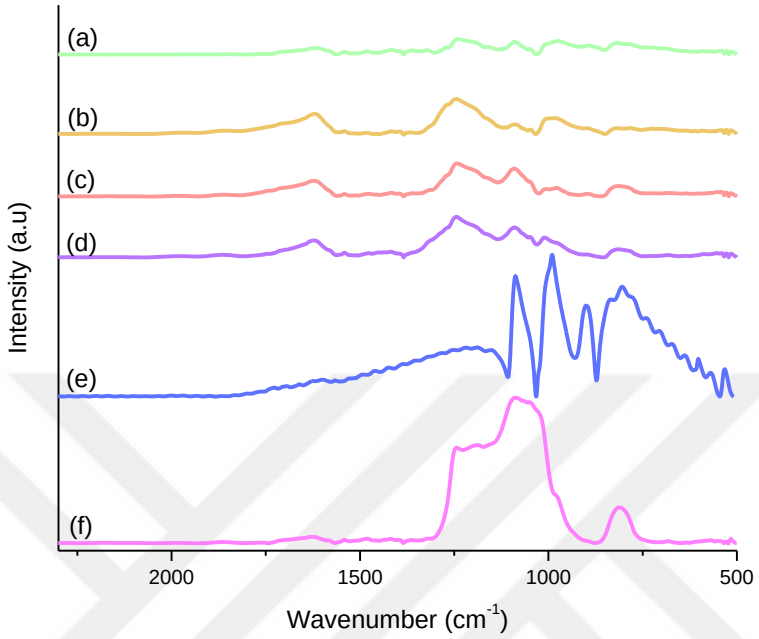

Fig. 5.2 FTIR spectra of SACs with a TPA loading of (a) 30 wt%; (b) 40 wt%; (c) 60 wt%; (d) 80 wt%; and of pristine (e) TPA, (f) MCM-41.

Next, we focused on determining the acid site density in each SAC by NH_3-TPD measurements.

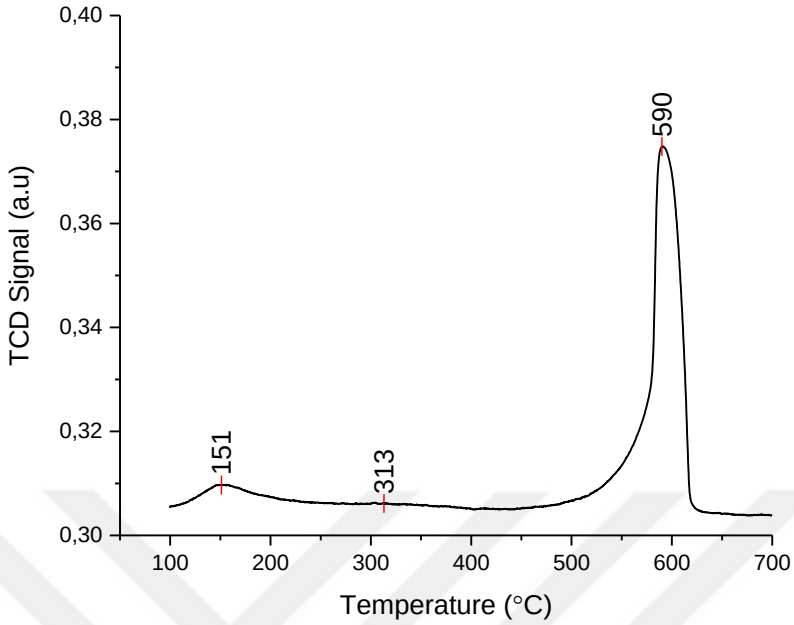

Fig. 5.3 NH_3-TPD profile of the as-received TPA obtained (under a helium flow of 50 cm^3min^{-1} with ramp of 3 °C min^{-1}).

The NH_3 desorption profile of the as-received TPA given in Fig. 5.3 shows three different peaks. Data suggest that the TPA cluster has acid sites with different acidic properties characterized by small and broad two peaks centered at 151 and 313 °C, followed by another sharp peak at 590 °C. The supported TPA samples were also characterized by similar peaks as summarized in Table 5.2. Because MeOH dehydration into DME on HPAs was reported to be favored on weak acid sites [56], we considered the variation of acid sites associated with the low temperature (LT) desorption peak.

Table 5.2 Determined acid sites peak positions and number of acid sites of the SACs determined by NH_3-TPD analysis.

Catalyst Loading (%)	Low Temperature Desorption Peak (°C)	Number of Acid Sites Determined from LT Desorption Peak ($mmolH^+/g$)
30	176	0.103
40	174	0,154
60	173	0.174
80	178	0.157
100	151	0.129

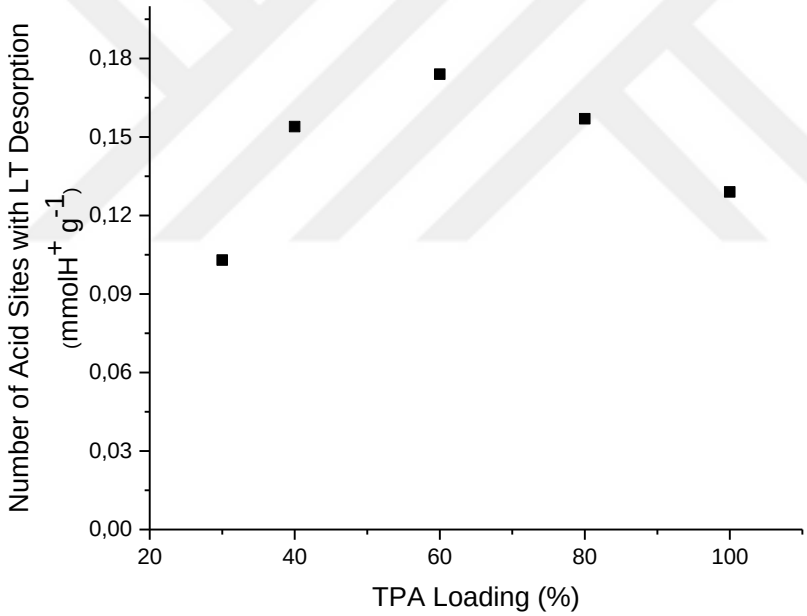

Fig. 5.4 Variation of the number of acid sites by low temperature desorption with the corresponding TPA loading.

Fig. 5.4 presents the variation of the number of acid sites associated with low temperature desorption peaks with increasing TPA loading in the corresponding SAC. The data show a volcano-type variation giving a peak at a TPA loading of 60 wt%. According to Kocaman et al. [49], the average TPA thickness rises exponentially if the TPA loading exceeds

50 wt%, suggesting a multilayer formation at significantly high TPA loadings. Consistently, our data indicate the presence of a monolayer TPA on the surface of the MCM-41 up to a TPA loading of 60 wt%. The consequent decrease in acid site density at a TPA loading of 80 wt% is associated with the coverage of acid site with as a second layer.

5.2.2 Catalytic Performance Results

In the absence of any SAC addition, the commercial MSC was tested for CO_2 hydrogenation at 250 °C and 45 bar and at a space velocity of 40 000 mL CO_2 $g_{cat}^{-1}h^{-1}$. Data suggested a CO_2 conversion of 9.2% producing MeOH and CO with the corresponding selectivities of 41.1% and 58.9%, respectively. When the MSC was mixed with SAC with a TPA loading of 40 wt.% at a mixing ratio of MSC:SAC = 3:1, the CO_2 conversion decreased from 9.2 to 5.8% at the same space velocity of 40 000 mL CO_2 $g_{cat}^{-1}h^{-1}$, where g_{cat} represents the total weight of the physical mixture (200 mg). The product analysis indicated a decrease in MeOH selectivity to 17.1% and a slight increase in the selectivity of CO to 63.9%. The data further indicated the presence of DME in the product stream with a selectivity of 19%. We infer that the decrease in the selectivity of methanol was associated with its subsequent conversion into DME on the SAC present in the physical mixture (Fig. 5.5).

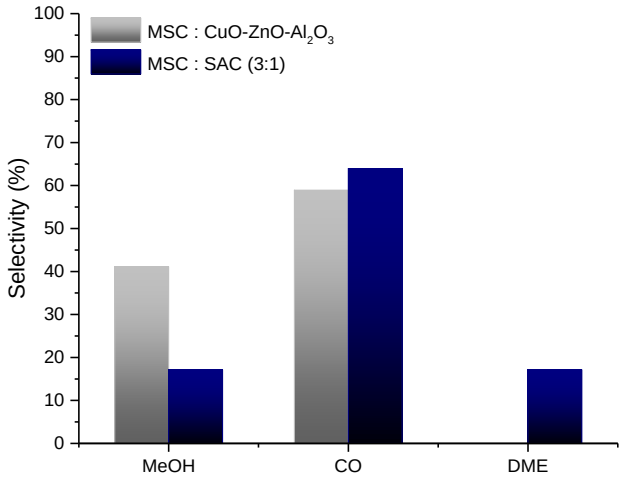

Fig. 5.5 Effect of acid function (SAC) addition (45 bar; H_2:CO_2, 3:1; GHSV, 40 000 mL CO_2 g_{cat}^{-1} h^{-1}; MSC:SAC, 3:1; SAC, 40:60 (wt:wt))

Fig. 5.6 demonstrates the variation of these results with temperature in a range from 220 to 250 °C at 45 bar and at a constant space velocity of 40 000 mL CO_2 g_{cat}^{-1} h^{-1} on the same physical mixture. In Fig.5.6 (B) the conversion of CO_2 tends to increase linearly with temperature, as expected. Thermodynamically, being an exothermic reaction, it is more favorable to synthesize DME at a lower reaction temperature [57]. This inference is consistent with the report of Shen et al. [58] demonstrating DME equilibrium yields decreased with temperature for any feed composition of H_2:CO_2. Consistently, our data showed that a decrease in reaction temperature resulted in an increase in DME selectivity from 19% at 250 °C to 25% at 220 °C. On the other hand, the CO selectivity rapidly increases from 25.5% at 220 °C to 63.9% at 250 °C. We infer that such a high CO production at high temperatures is mainly associated with the contribution of the endothermic reverse water gas shift (RWGS) reaction [59]. In other words, this trend can be explained as follows: under the conditions of CO_2 hydrogenation, two competing reactions consume CO_2, one is the synthesis of dehydration of MeOH and the other one is the RWGS reaction, a progressive increase of the reaction temperature leads to an increase in the equilibrium conversion of the endothermic RWGS reaction [60]. Overall, when considering the DME production rate in Fig.5.6 (B), the space time yield of DME (STY_{DME}) shows a progressive increase as a function of reaction temperature reaching a maximum value of 834.4 g_{DME} kg^{-1} h^{-1} at 250 °C [58]. Thus, we set the reaction temperature to 250 °C, as it provides the highest DME production rate compared to lower temperatures, even though the selectivity for DME was not the highest at this temperature. Here, we note that because we activated our catalysts at 250 °C, we set the maximum temperature for our operation to 250 °C.

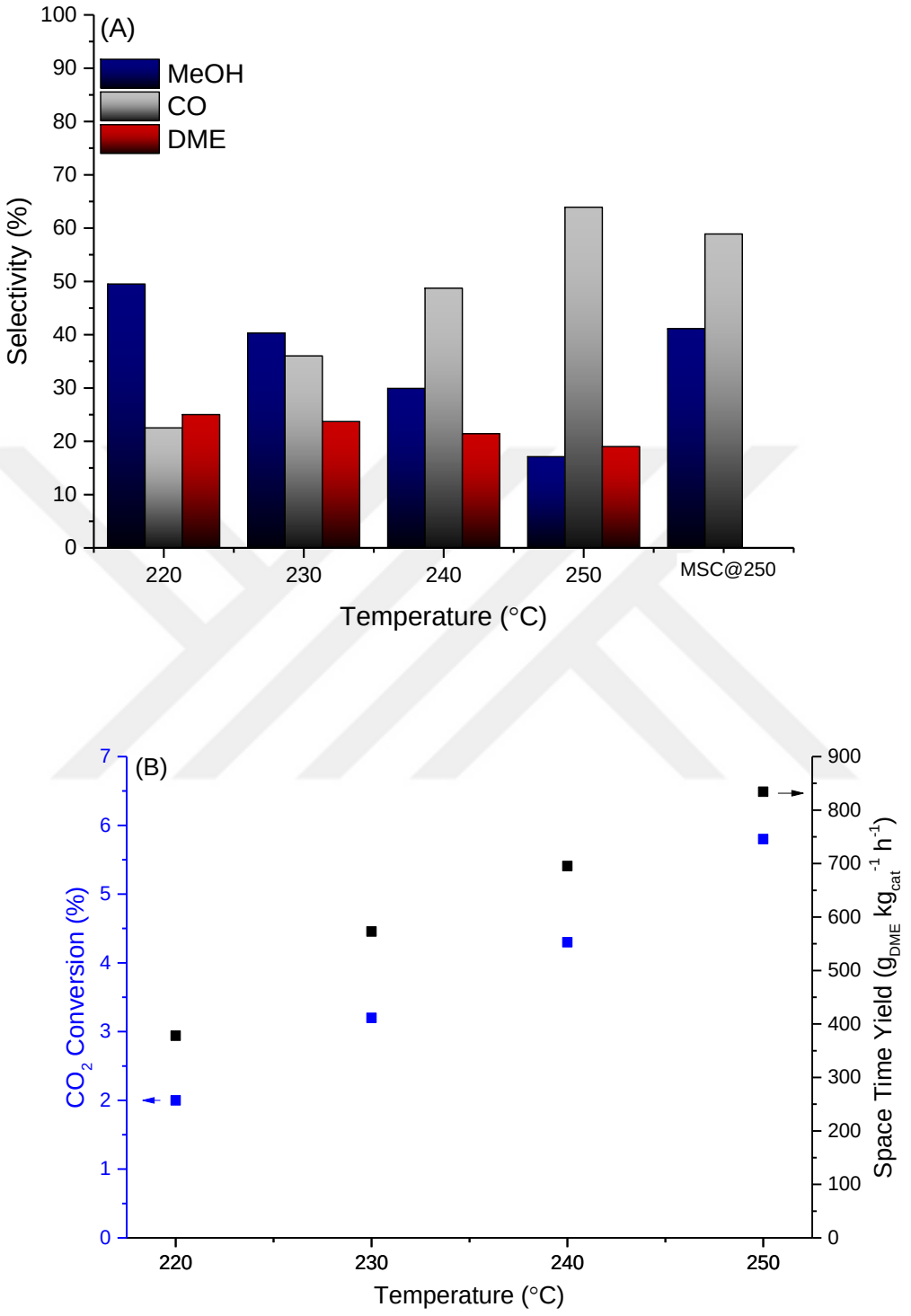

Fig. 5.6 Influence of reaction temperature A) on product selectivity (MSC@250 means that as-received commercial catalyst was performed at 250 °C using (45 bar; H_2:CO_2, 3:1; GHSV, 40 000 mL CO_2 $g_{cat}^{-1}h^{-1}$) B) on STY_{DME} (45 bar; H_2:CO_2, 3:1; GHSV, 40 000 mL CO_2 $g_{cat}^{-1}h^{-1}$; MSC:SAC=3:1, SAC, 40:60 (wt:wt)).

To optimize the DME production rate further, the effect of space velocity on the activity–selectivity pattern of the MSC:SAC (3:1, wt:wt) with a SAC having a TPA loading of 40 wt% was investigated by varying the space velocity from 40 000-7 000 mL CO_2 g_{cat}^{-1} h^{-1} at 250 °C and 45 bar. Fig. 5.7 summarizes the results of these measurements. Data showed that as the space velocity decreases from 40 000 to 7 000 mL CO_2 g_{cat}^{-1} h^{-1}, the CO_2 conversion increases from 5.8 to 12.8% (Fig.5.7. (A)), as expected. On the other hand, Fig.5.7 (B) illustrates the influence of space velocity on the product distribution. Accordingly, the DME selectivity increases from 13.8 to 19.0% with a decrease in CO selectivity from 76.0 to 63.9% with increasing space velocity. Fig.5.7 (A) further demonstrates the variation of STY_{DME} with increasing space velocity. Accordingly, the STY_{DME} increases from approximately 233.2 mL CO_2 g_{cat}^{-1} h^{-1} to 834.4 mL CO_2 g_{cat}^{-1} h^{-1} as the space velocity increases from 7000 to 40 000 mL CO_2 g_{cat}^{-1} h^{-1}. This increase in STY_{DME} with space velocity is consistent with the report of Bonura et al. [61]. Based on these results, we set the space velocity as the highest value that we can reach within our limitations (40 000 mL CO_2 g_{cat}^{-1} h^{-1}) to be able to reach the highest DME production rate.

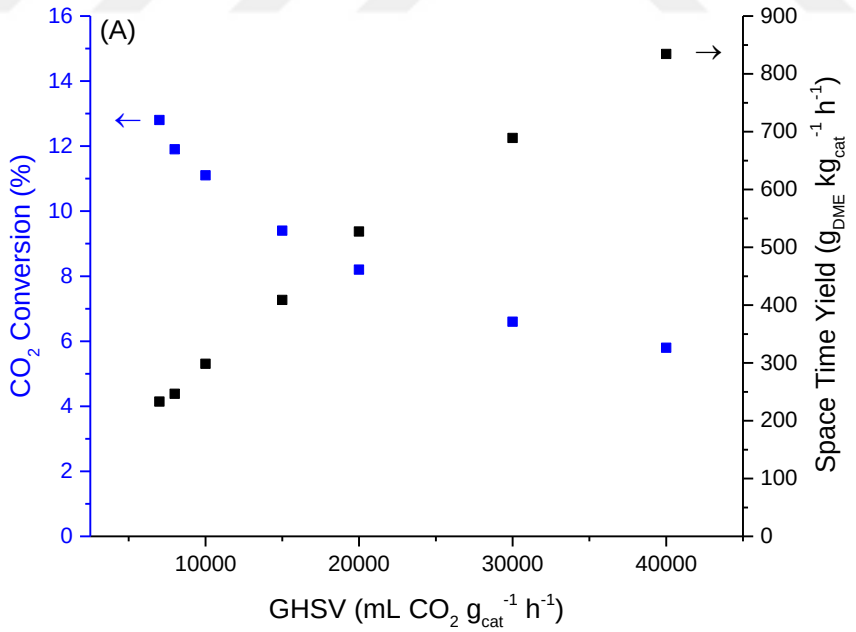

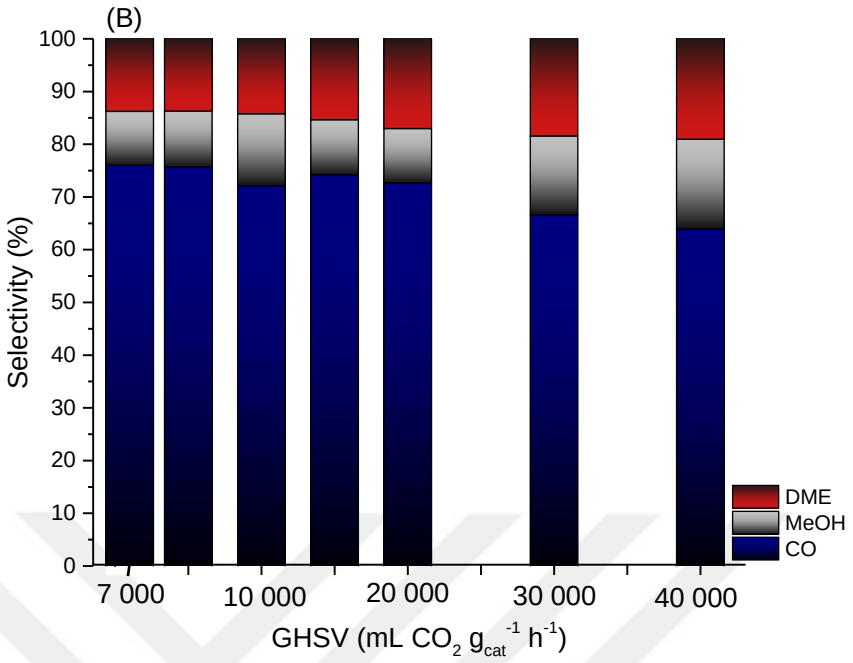

Fig. 5.7 Influence of space velocity on (A) CO_2 conversion and STY_{DME} and (B) on selectivity, (at 250 °C; 45 bar; H_2:CO_2, 3:1; MSC: SAC=3:1, SAC, 40:60 (wt:wt), where g_{cat} represents the total amount of the physical mixture).

Next, we focused on optimizing the ratio of MSC amount over SAC amount present in the physical mixture for high STY_{DME}. Fig. 5.8 shows the variation of CO_2 conversion, product selectivities, and STY_{DME} with varying MSC:SAC ratios of 2:1, 3:1, and 4:1 (wt:wt) at a fixed total amount of physical mixture of 0.2 g and a fixed space velocity of 40 000 mL CO_2 g_{cat}^{-1} h^{-1}. Accordingly, as the ratio of MSC:SAC in the physical mixture increases, the CO_2 conversion also increases, as expected. However, this gradual increasing trend in CO_2 conversion was not valid on the product selectivities. Figure 5.8 (B) shows that the selectivities for MeOH, CO, and DME first changed from 19, 56.7, 24.3% to 17.1, 63.9, 19% respectively, with an increase in MSC:SAC ratio from 2:1 to 3:1. As the ratio further increases to 4:1, the corresponding selectivities were 33.6, 37.3 and 29.1% respectively. These changes in product selectivities suggest changes in STY_{DME} as presented in Fig 5.8 (A). Accordingly, the STY_{DME} reaches a maximum value of 1340.0 g_{DME} kg^{-1} h^{-1}at an MSC:SAC ratio of 4:1.

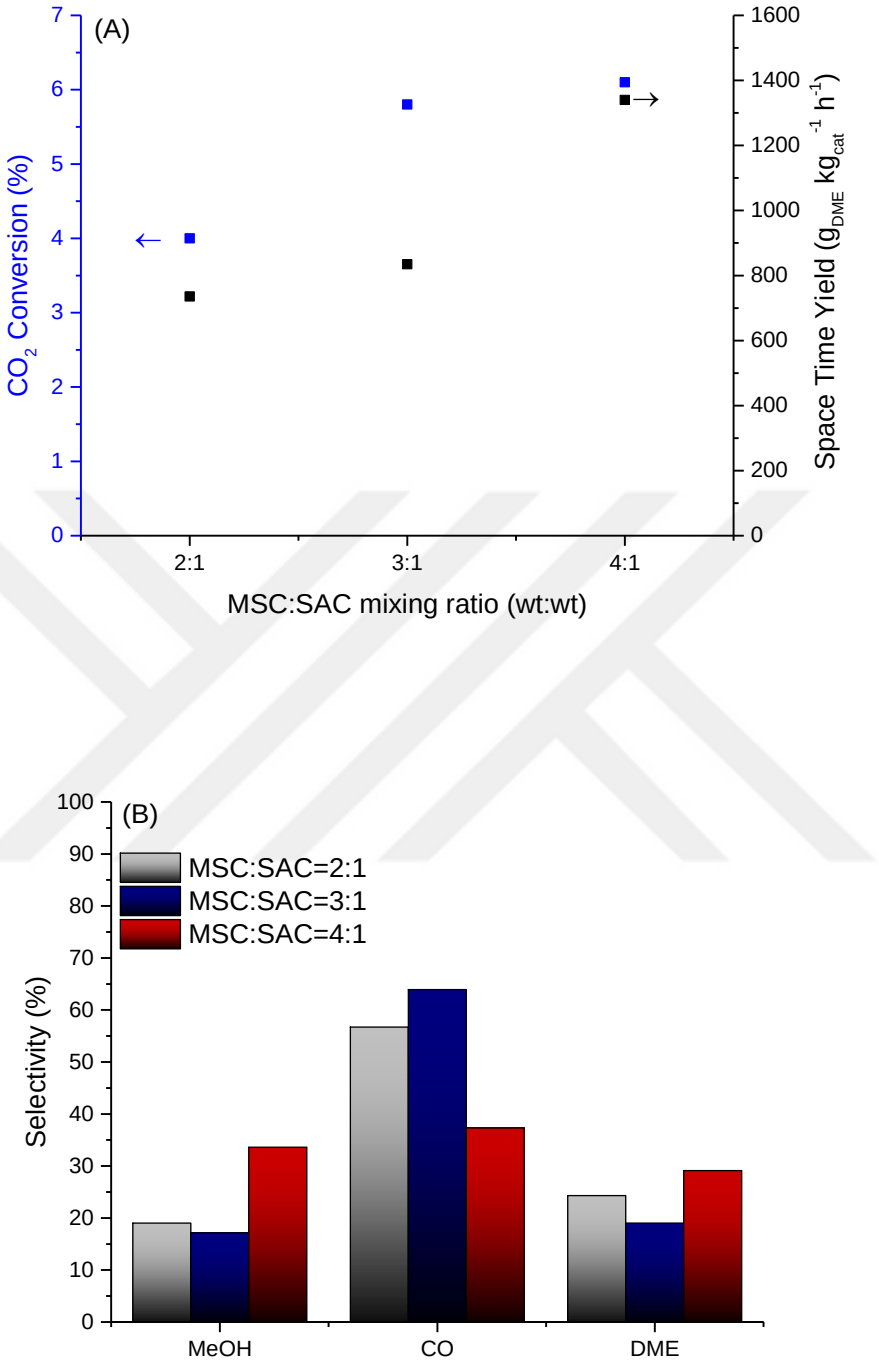

Fig. 5.8. Effect of MSC:SAC mixing ratio A) on CO_2 conversion and STY_{DME} (B) on product selectivity (250 °C; 45 bar, H_2:CO_2, 3:1; GHSV, 40 000 mL CO_2 $g_{cat}^{-1}h^{-1}$; SAC, 40:60 (wt:wt)).

These results demonstrated that the ratio of MSC:SAC in the physical mixture is an important parameter in determining the STY_{DME}. Having a higher amount of MSC in the mixture helps to maintain a higher amount of CO_2 conversion; however, this approach reduces the amount of acid sites available for dehydrating MeOH product in the catalyst bed. One way of increasing the number of available acid sites without compromising from high MSC:SAC ratios is increasing the TPA loading in the SAC. To investigate the effect of TPA loading in SAC catalyst we set the MSC:SAC ratio to 4:1 and varied the TPA loading in SAC and tested the performance of the physical mixture at 250 °C and 45 bar with a space velocity of 40 000 mL CO_2 g_{cat}^{-1} h^{-1}. Fig. 5.9 demonstrates the results of these measurements. Data showed that the lowest CO_2 conversion was at 30 wt%, might be associated with strong structural distortions on the TPA clusters as indicated by the FTIR and XRD results. Fig. 8 (A) further showed that the CO_2 conversion first increased from 5.5 to 8.9% with an increase in TPA loading from 30 to 60 wt%, however it then decreased 7% when the TPA loading was further increased to 80 wt%. At this highest TPA loading considered, the DME selectivity was the lowest (18.2%). The decrease in CO_2 conversion and DME selectivity with an increase in TPA loading from 60 to 80 wt% might be related with the inaccessibility of the acid sites because of the accumulation or multilayer formation of the TPA clusters at these extremely high TPA loadings [49]. Besides, Raimando et al. studied the structure-activity relationships on different Al_2O_3-based acid catalysts and concluded that dehydration was preferred in larger pores [62]. Thus, we infer that this decrease in dehydration performance at 80 wt% TPA loading might also be related with the decrease in pore volume with the increase in TPA loading, as shown above.

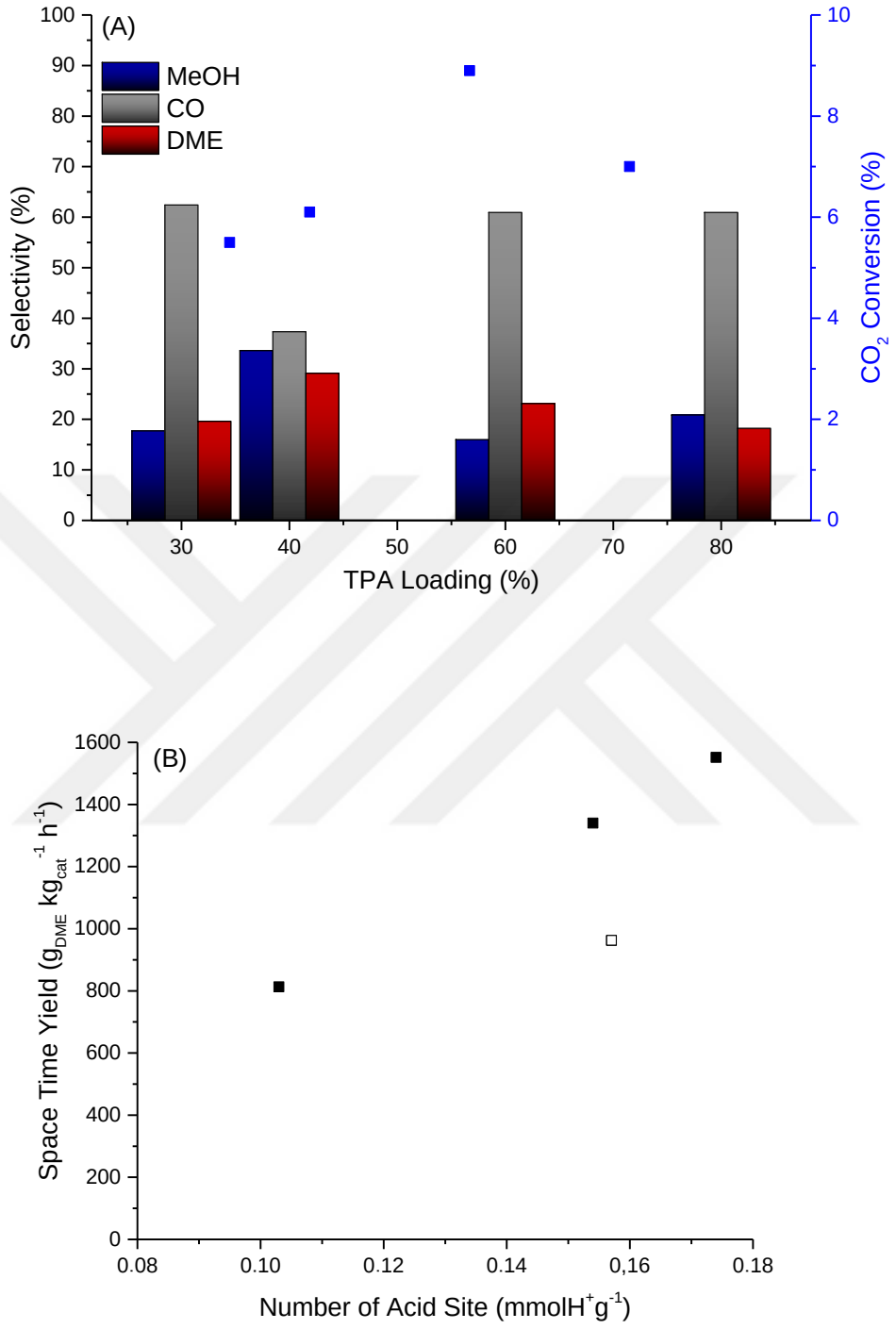

Fig. 8. A) Effect of TPA loading on product selectivity and CO_2 conversion; B) effect of number of acid site on STY_{DME} (T_R, 250 °C; P_R, 45 bar, H_2:CO_2, 3:1; GHSV, 40 000 mL CO_2 $g_{cat}^{-1}h^{-1}$; MSC:SAC= 4:1). Acid catalyst with TPA loading at 80 wt% is shown with open symbols (□).

Aiming at elucidating the links between the acid characteristics of these catalysts and the corresponding STY_{DME}, we considered the variation of STY_{DME} with increasing acid site density. Fig. 5.9 (B) illustrates that STY_{DME} increases linearly with the amount of acid sites. Data present a perfect correlation with an R^2 value of 1.0, when only the SAC catalysts with a monolayer distribution of TPA clusters are considered. Based on these results we infer that the number of active acid sites directly available for the dehydration of MeOH is another important factor influencing the STY_{DME}. In this respect, the MCM-41 support offers an excellent platform for the monolayer dispersion of TPA clusters even at an extremely high TPA loading of 60 wt% owing to its exceptionally high surface area.

Table 5.3 presents a comparison of STY_{DME} values with the literature. The comparison indicates that the STY_{DME} value of 1551.5 g_{DME} kg^{-1} h^{-1} presented here in Fig. 5.9(B) obtained on a physical mixture of MSC:SAC prepared at a mixing ratio of 4:1 (wt:wt) including 60 wt% TPA-loaded SAC is, to the best of our knowledge, more than twice of the highest value ever reported for the direct conversion of CO_2 into DME [45]. We note that the MSC that we considered here is optimized specifically for the conversion of synthesis gas, and thus, we envision that the STY_{DME} can be improved even further when the supported TPA catalysts that is presented here is used together with a methanol synthesis catalyst specifically designed for high performance in CO_2 hydrogenation.

Table 5.3 Summary of the catalysts reported for the direct hydrogenation of CO_2 to DME.

Catalyst	T (°C)	P (bar)	$H_2/CO_2/N_2$	GHSV ($ml_{CO2}g_{cat}^{-1}h^{-1}$)	X_{CO2} (%)	S_{DME} (%)	STY_{DME} ($g_{DME}kg_{cat}^{-1}h^{-1}$)	Ref.
Cu-Zn-Zr/FER	260	50	9/3/1	2030	26	55.7	600	[33]
Cu-Zn-Zr/FER	280	50	9/3/1	2030	30	62	752	[45]
CuO-Fe_2O_3-ZrO_2/HZSM-5	260	30	5/1	250	28.4	64.5	86	[37]
PdZn/TiO_2/ZSM-5	270	20	3/1/1	720	11	32.3	48	[63]
Cu-ZnO-ZrO_2/HZSM-5	243	30	9/3/1	2076	15	25	147	[61]
CuO-ZnO-ZrO_2/WO_x/Al_2O_3	260	30	9/3/1	3000	18.9	15.3	164	[64]
CuO-ZnO-Al_2O_3/HZSM-5	260	30	9/3/1	346	27.3	67.1	120	[34]
CuO-ZnO-ZrO_2/WO_x/ZrO_2	260	30	9/3/1	1000	21.5	29	271	[65]
Cu-Zn-Zr/MFI	240	50	9/3/1	2307	24	49.3	513	[31]
Cu-Zn-Ga/FER	260	30	9/3/1	2030	21.1	34.9	282	[60]
Cu-Zn-Al/HZSM-5	260	50	3/1	750	31	65	285	[66]
Cu-Zn-Al/Al_2O_3	260	50	3/1	750	20	82	232	[66]

Cu-Zn-Al-Zr/ZSM-5	260	30	3/1	400	25	23.3	43	[67]
Cu-Zn-Al/ZSM-5+CNTs	260	30	3/1	450	46.2	45.2	177	[68]
CuO-ZnO-ZrO_2/SO_4^{2-}-ZrO_2	260	20	9/3/1	3750	17.2	25.6	311	[69]
CuO-ZnO-Al_2O_3/HZSM-5	260	42	3/1	381	30.5	72	158	[70]
Cu-Zn-Zr-V/ZSM-5	270	30	3/1	1050	32.3	57.8	370	[43]
Cu-Zn-Zr-Pd/ZSM-5	200	30	3/1	450	18.7	73.6	117	[39]
CuO-TiO_2-ZrO_2/HZSM-5	250	30	3/1	375	15.6	47.5	52	[41]
Cu-Zn-Al-La/HZSM-5	250	30	3/1	750	43.8	71.2	441	[71]
Cu/Zn/Al Amorphous Si-Al	266	30	3/1	450	47.1	42.4	170	[72]
Cu-Mo/HZSM-5	240	20	3/1	375	12.4	77.2	68	[73]
CuO-Fe_2O_3-CeO_2/HZSM-5	260	30	4/1	375	20.9	63.1	93	[44]
Cu-Fe-Ce/HZSM-5	260	30	4/1	375	18.1	52	67	[38]
Cu-Fe-La/HZSM-5	260	30	4/1	375	17.2	51.3	62	[38]
CuO-ZnO-Al_2O_3:TPA/MCM-4	250	45	3/1	40 000	8.9	23.1	1551.5	This work

References

[1] R. Lal, Sequestration of atmospheric CO2 in global carbon pools, Energy & Environmental Science, 1 (2008) 86.

[2] M.D. Porosoff, B. Yan, J.G. Chen, Catalytic reduction of CO_2 by H_2 for synthesis of CO, methanol and hydrocarbons: Challenges and opportunities, Energy and Environmental Science, 9 (2016) 62-73.

[3] S. Saeidi, N.A.S. Amin, M.R. Rahimpour, Hydrogenation of CO_2 to value-added products - A review and potential future developments, Journal of CO_2 Utilization, 5 (2014) 66-81.

[4] G. Centi, S. Perathoner, Opportunities and prospects in the chemical recycling of carbon dioxide to fuels, Catalysis Today, 148 (2009) 191-205.

[5] Y.H. Choi, Y.J. Jang, H. Park, W.Y. Kim, Y.H. Lee, S.H. Choi, J.S. Lee, Carbon dioxide Fischer-Tropsch synthesis: A new path to carbon-neutral fuels, Applied Catalysis B: Environmental, 202 (2017) 605-610.

[6] K.A. Ali, A.Z. Abdullah, A.R. Mohamed, Recent development in catalytic technologies for methanol synthesis from renewable sources: A critical review, Renewable and Sustainable Energy Reviews, 44 (2015) 508-518.

[7] S.G. Jadhav, P.D. Vaidya, B.M. Bhanage, J.B. Joshi, Catalytic carbon dioxide hydrogenation to methanol: A review of recent studies, Chemical Engineering Research and Design, 92 (2014) 2557-2567.

[8] G.A. Olah, Beyond oil and gas: The methanol economy, Angewandte Chemie - International Edition, 44 (2005) 2636-2639.

[9] A. Goeppert, M. Czaun, J.P. Jones, G.K. Surya Prakash, G.A. Olah, Recycling of carbon dioxide to methanol and derived products - closing the loop, Chem Soc Rev, 43 (2014) 7995-8048.

[10] I.U. Din, M.S. Shaharun, M.A. Alotaibi, A.I. Alharthi, A. Naeem, Recent developments on heterogeneous catalytic CO_2 reduction to methanol, Journal of CO_2 Utilization, 34 (2019) 20-33.

[11] U. Olsbye, S. Svelle, M. Bjorgen, P. Beato, T.V. Janssens, F. Joensen, S. Bordiga, K.P. Lillerud, Conversion of methanol to hydrocarbons: how zeolite cavity and pore size controls product selectivity, Angew Chem Int Ed Engl, 51 (2012) 5810-5831.

[12] Recent trends and fundamental insights in the methanol-to-hydrocarbons process.

[13] Z. Li, J. Wang, Y. Qu, H. Liu, C. Tang, S. Miao, Z. Feng, H. An, C. Li, Highly Selective Conversion of Carbon Dioxide to Lower Olefins, ACS Catalysis, 7 (2017) 8544-8548.

[14] J. Wei, Q. Ge, R. Yao, Z. Wen, C. Fang, L. Guo, H. Xu, J. Sun, Directly converting CO_2 into a gasoline fuel, Nature Communications, 8 (2017) 15174.

[15] P. Gao, S. Li, X. Bu, S. Dang, Z. Liu, H. Wang, L. Zhong, M. Qiu, C. Yang, J. Cai, W. Wei, Y. Sun, Direct conversion of CO_2 into liquid fuels with high selectivity over a bifunctional catalyst, Nat Chem, 9 (2017) 1019-1024.

[16] Y. Ni, Z. Chen, Y. Fu, Y. Liu, W. Zhu, Z. Liu, Selective conversion of CO2 and H2 into aromatics, Nat Comm, 9 (2018) 3457

[17] O. Martin, A.J. Martin, C. Mondelli, S. Mitchell, T.F. Segawa, R. Hauert, C. Drouilly, D. Curulla-Ferre, J. Perez-Ramirez, Indium Oxide as a Superior Catalyst for Methanol Synthesis by CO_2 Hydrogenation, Angew Chem Int Ed Engl, 55 (2016) 6261-6265.

[18] J. Sun, G. Yang, Y. Yoneyama, N. Tsubaki, Catalysis Chemistry of Dimethyl Ether Synthesis, ACS Catalysis, 4 (2014) 3346-3356.

[19] E. Catizzone, G. Bonura, M. Migliori, F. Frusteri, G. Giordano, CO_2 Recycling to Dimethyl Ether: State-of-the-Art and Perspectives, Molecules, 23 (2017).

[20] Z. Azizi, M. Rezaeimanesh, T. Tohidian, M.R. Rahimpour, Dimethyl ether: A review of technologies and production challenges, Chemical Engineering and Processing: Process Intensification, 82 (2014) 150-172.

[21] G. Olah, A. Goeppert, and G. K. S.Prakash, Chemical Recycling of Carbon Dioxide to Methanol and Dimethyl, 74, J. Org. Chem. (2009), 487–498

[22] M. Marchionna, R. Patrini, D. Sanfilippo, G. Migliavacca, Fundamental investigations on di-methyl ether (DME) as LPG substitute or make-up for domestic uses, Fuel Processing Technology, 89 (2008) 1255-1261.

[23] C. Arcoumanis, C. Bae, R. Crookes, E. Kinoshita, The potential of di-methyl ether (DME) as an alternative fuel for compression-ignition engines: A review, Fuel, 87 (2008) 1014-1030.

[24] R. Ahmad, D. Schrempp, S. Behrens, J. Sauer, M. Döring, U. Arnold, Zeolite-based bifunctional catalysts for the single step synthesis of dimethyl ether from CO-rich synthesis gas, Fuel Processing Technology, 121 (2014) 38-46.

[25] R. Khoshbin, M. Haghighi, Direct syngas to DME as a clean fuel: The beneficial use of ultrasound for the preparation of CuO-ZnO-Al_2O_3/HZSM-5 nanocatalyst, Chemical Engineering Research and Design, 91 (2013) 1111-1122.

[26] R. Nie, H. Lei, S. Pan, L. Wang, J. Fei, Z. Hou, Core–shell structured CuO–ZnO@H-ZSM-5 catalysts for CO hydrogenation to dimethyl ether, Fuel, 96 (2012) 419-425.

[27] Q.X.-M. Gong-Xin, Zheng; Jin-Hua, Fei; Zhao-Yin, Hou, A novel catalyst for DME synthesis from CO hydrogenation 1. Activity, structure and surface properties.pdf, Journal of Molecular Catalysis A: Chemical, 176 (2001) 195–203.

[28] S. Asthana, C. Samanta, A. Bhaumik, B. Banerjee, R.K. Voolapalli, B. Saha, Direct synthesis of dimethyl ether from syngas over Cu-based catalysts: Enhanced selectivity in the presence of MgO, Journal of Catalysis, 334 (2016) 89-101.

[29] S.S. Akarmazyan, P. Panagiotopoulou, A. Kambolis, C. Papadopoulou, D.I. Kondarides, Methanol dehydration to dimethylether over Al_2O_3 catalysts, Applied Catalysis B: Environmental, 145 (2014) 136-148.

[30] A.R. de la Osa, A. Romero, J. Díez-Ramírez, J.L. Valverde, P. Sánchez, Influence of a Zeolite-Based Cascade Layer on Fischer–Tropsch Fuels Production over Silicon Carbide Supported Cobalt Catalyst, Topics in Catalysis, (2017) 1-12.

[31] F. Frusteri, G. Bonura, C. Cannilla, G. Drago Ferrante, A. Aloise, E. Catizzone, M. Migliori, G. Giordano, Stepwise tuning of metal-oxide and acid sites of CuZnZr-MFI hybrid

catalysts for the direct DME synthesis by CO_2 hydrogenation, Applied Catalysis B: Environmental, 176-177 (2015) 522-531.

[32] F. Frusteri, M. Cordaro, C. Cannilla, G. Bonura, Multifunctionality of Cu-ZnO-ZrO2/H-ZSM5 catalysts for the one-step CO_2-to-DME hydrogenation reaction, Applied Catalysis B: Environmental, 162 (2015) 57-65.

[33] F. Frusteri, M. Migliori, C. Cannilla, L. Frusteri, E. Catizzone, A. Aloise, G. Giordano, G. Bonura, Direct CO_2-to-DME hydrogenation reaction: New evidences of a superior behaviour of FER-based hybrid systems to obtain high DME yield, Journal of CO_2 Utilization, 18 (2017) 353-361.

[34] Y. Hu, Y. Zhang, J. Du, C. Li, K. Wang, L. Liu, X. Yu, K. Wang, N. Liu, The influence of composition on the functionality of hybrid CuO-ZnO-Al_2O_3/HZSM-5 for the synthesis of DME from CO_2 hydrogenation, RSC Advances, 8 (2018) 30387-30395.

[35] J.-H. Kim, M.J. Park, S.J. Kim, O.-S. Joo, K.-D. Jung, DME synthesis from synthesis gas on the admixed catalysts of Cu/ZnO/Al_2O_3 and ZSM-5, Applied Catalysis A: General, 264 (2004) 37-41.

[36] L. Li, D. Mao, J. Xiao, L. Li, X. Guo, J. Yu, Facile preparation of highly efficient CuO-ZnO-ZrO_2/HZSM-5 bifunctional catalyst for one-step CO_2 hydrogenation to dimethyl ether: Influence of calcination temperature, Chemical Engineering Research and Design, 111 (2016) 100-108.

[37] R.W. Liu, Z.Z. Qin, H.B. Ji, T.M. Su, Synthesis of dimethyl ether from CO_2 and H_2 using a Cu-Fe-Zr/HZSM-5 catalyst system, Industrial and Engineering Chemistry Research, 52 (2013) 16648-16655.

[38] Z.Z. Qin, X.H. Zhou, T.M. Su, Y.X. Jiang, H.B. Ji, Hydrogenation of CO_2 to dimethyl ether on La-, Ce-modified Cu-Fe/HZSM-5 catalysts, Catalysis Communications, 75 (2016) 78-82.

[39] K. Sun, W. Lu, M. Wang, X. Xu, Low-temperature synthesis of DME from CO2/H2 over Pd-modified CuO-ZnO-Al_2O_3-ZrO_2/HZSM-5 catalysts, Catalysis Communications, 5 (2004) 367-370.

[40] H. Wang, Y. Wang, W. Gao, W. Guo, M. Jia, Dimethyl ether synthesis from CO_2 hydrogenation on La-modified CuO-ZnO-Al_2O_3/HZSM-5 bifunctional catalysts, Journal of Rare Earths, 31 (2013) 470-476.

[41] S. Wang, D. Mao, X. Guo, G. Wu, G. Lu, Dimethyl ether synthesis via CO2 hydrogenation over CuO-TiO_2-ZrO_2/HZSM-5 bifunctional catalysts, Catalysis Communications, 10 (2009) 1367-1370.

[42] K.S. Yoo, J.-H. Kim, M.-J. Park, S.-J. Kim, O.-S. Joo, K.-D. Jung, Influence of solid acid catalyst on DME production directly from synthesis gas over the admixed catalyst of Cu/ZnO/Al_2O_3 and various SAPO catalysts, Applied Catalysis A: General, 330 (2007) 57-62.

[43] Y. Zhang, D. Li, Y. Zhang, Y. Cao, S. Zhang, K. Wang, F. Ding, J. Wu, V-modified CuO-ZnO-ZrO_2/HZSM-5 catalyst for efficient direct synthesis of DME from CO_2 hydrogenation, Catalysis Communications, 55 (2014) 49-52.

[44] X. Zhou, T. Su, Y. Jiang, Z. Qin, H. Ji, Z. Guo, CuO-Fe_2O_3-CeO_2/HZSM-5 bifunctional catalyst hydrogenated CO_2 for enhanced dimethyl ether synthesis, Chemical Engineering Science, 153 (2016) 10-20.

[45] G. Bonura, F. Frusteri, C. Cannilla, G. Drago Ferrante, A. Aloise, E. Catizzone, M. Migliori, G. Giordano, Catalytic features of CuZnZr–zeolite hybrid systems for the direct CO_2-to-DME hydrogenation reaction, Catalysis Today, 277 (2016) 48-54.

[46] M.H. Zhang, Z.M. Liu, G.D. Lin, H.B. Zhang, Pd/CNT-promoted $CuZrO_2$/HZSM-5 hybrid catalysts for direct synthesis of DME from CO_2/H_2, Applied Catalysis A: General, 451 (2013) 28-35.

[47] I. V. Kozhevnikov, Catalysis by Heteropoly Acids and Multicomponent Polyoxometalates in Liquid-Phase Reactions, Chemical Reviews, 98 (1998), 171-198

[48] W. Alharbi, E.F. Kozhevnikova, I.V. Kozhevnikov, Dehydration of Methanol to Dimethyl Ether over Heteropoly Acid Catalysts: The Relationship between Reaction Rate and Catalyst Acid Strength, ACS Catalysis, 5 (2015) 7186-7193.

[49] E. Kocaman, Ö. Akarçay, N. Bağlar, S. Çelebi, A. Uzun, Isobutene oligomerization on MCM-41-supported tungstophosphoric acid, Molecular Catalysis, 457 (2018) 41-50.

[50] P.J.R. Shyam Kattel, Jingguang G. Chen, José A. Rodriguez, Ping Liu, Active sites for CO_2 hydrogenation to methanol on Cu/ZnO catalysts, Science 336 (2012) 893–897.

[51] F.S. Malte Behrens, Igor Kasatkin,Stefanie Kühl, Michael Hävecker,, S.Z. Frank Abild-Pedersen, Frank Girgsdies, Patrick Kurr, Benjamin-Louis Kniep, R.W.F. Michael Tovar, Jens K. Nørskov, Robert Schlögl, The Active Site of Methanol Synthesis over Cu/ZnO/Al_2O_3 industrial catalysts, Science 336 (2012) 893–897.

[52] A.D. Newman, D.R. Brown, P. Siril, A.F. Lee, K. Wilson, Structural studies of high dispersion $H_3PW_{12}O_{40}$/SiO_2 solid acid catalysts, Phys Chem Chem Phys, 8 (2006) 2893-2902.

[53] A.K. Dizaji, B. Mokhtarani, H.R. Mortaheb, Deep and fast oxidative desulfurization of fuels using graphene oxide-based phosphotungstic acid catalysts, Fuel, 236 (2019) 717-729.

[54] J. Zhang, M. Kanno, Y. Wang, H. Nishii, Y.-k. Miura, Y. Kamiya, Changes in Surface Acidity of Silica-Supported Dodecatungstosilicic Acid in Relation to the Loading Amount, The Journal of Physical Chemistry C, 115 (2011) 14762-14769.

[55] F.J. Berry, G.R. Derrick, J.F. Marco, M. Mortimer, Silica-supported silicotungstic acid: A study by X-ray photoelectron spectroscopy, Materials Chemistry and Physics, 114 (2009) 1000-1003.

[56] J.J. Spivey, Review: Dehydration Catalysts for the Methanol/Dimethyl Ether Reaction, Chemical Engineering Communications, 110 (2010) 123-142.

[57] G. Bonura, M. Cordaro, L. Spadaro, C. Cannilla, F. Arena, F. Frusteri, Hybrid Cu–ZnO–ZrO_2/H-ZSM5 system for the direct synthesis of DME by CO_2 hydrogenation, Applied Catalysis B: Environmental, 140-141 (2013) 16-24.

[58] W. Shen, K.Jun , H.Choi, K. LeeThermodynamic investigation of methanol and dimethyl ether synthesis from CO_2 Hydrogenation, Korea.Chem. Eng., 2, (2000), 210-216

[59] K. Stangeland, H. Li, Z. Yu, Thermodynamic Analysis of Chemical and Phase Equilibria in CO2 Hydrogenation to Methanol, Dimethyl Ether, and Higher Alcohols, Industrial & Engineering Chemistry Research, 57 (2018) 4081-4094.

[60] G. Bonura, C. Cannilla, L. Frusteri, F. Frusteri, The influence of different promoter oxides on the functionality of hybrid CuZn-ferrierite systems for the production of DME from CO_2-H_2 mixtures, Applied Catalysis A: General, 544 (2017) 21-29.

[61] G. Bonura, M. Cordaro, C. Cannilla, A. Mezzapica, L. Spadaro, F. Arena, F. Frusteri, Catalytic behaviour of a bifunctional system for the one step synthesis of DME by CO_2 hydrogenation, Catalysis Today, 228 (2014) 51-57.

[62] M.Raimondo, A. Stefanis, G. Perez, A. Tomlinson, PLS vs. zeolites as sorbents and catalysts. 5. Evidence for BrønstedLewis acid crossover and high acidity in conversions of C1–3 alcohols in some alumina-pillared smectite clays. Applied Catalysis A: General 171 (1998) 85-97.

[63] H. Bahruji, R.D. Armstrong, J. Ruiz Esquius, W. Jones, M. Bowker, G.J. Hutchings, Hydrogenation of CO_2 to Dimethyl Ether over Brønsted Acidic PdZn Catalysts, Industrial & Engineering Chemistry Research, 57 (2018) 6821-6829.

[64] Y. Suwannapichat, T. Numpilai, N. Chanlek, K. Faungnawakij, M. Chareonpanich, J. Limtrakul, T. Witoon, Direct synthesis of dimethyl ether from CO_2 hydrogenation over novel

hybrid catalysts containing a Cu ZnO ZrO_2 catalyst admixed with WO_x/Al_2O_3 catalysts: Effects of pore size of Al_2O_3 support and W loading content, Energy Conversion and Management, 159 (2018) 20-29.

[65] T. Witoon, P. Kidkhunthod, M. Chareonpanich, J. Limtrakul, Direct synthesis of dimethyl ether from CO_2 and H_2 over novel bifunctional catalysts containing CuO-ZnO-ZrO_2 catalyst admixed with WO_x /ZrO_2 catalysts, Chemical Engineering Journal, 348 (2018) 713-722.

[66] S.P. Naik, T. Ryu, V. Bui, J.D. Miller, N.B. Drinnan, W. Zmierczak, Synthesis of DME from CO_2/H_2 gas mixture, Chemical Engineering Journal, 167 (2011) 362-368.

[67] Y. Zhao, Effects of ZrO_2 on the Performance of CuO-ZnO-Al_2O_3 HZSM-5 Catalyst for Dimethyl Ether Synthesis from CO_2 Hydrogenation, Journal of Natural Gas Chemistry 16 (2007) 389-392.

[68] F. Zha, H. Tian, J. Yan, Y. Chang, Multi-walled carbon nanotubes as catalyst promoter for dimethyl ether synthesis from CO2 hydrogenation, Applied Surface Science, 285 (2013) 945-951.

[69] C. Temvuttirojn, N. Chuasomboon, T. Numpilai, K. Faungnawakij, M. Chareonpanich, J. Limtrakul, T. Witoon, Development of SO_4^{2-}-ZrO_2 acid catalysts admixed with a CuO-ZnO-ZrO_2 catalyst for CO_2 hydrogenation to dimethyl ether, Fuel, 241 (2019) 695-703.

[70] S. Ren, W.R. Shoemaker, X. Wang, Z. Shang, N. Klinghoffer, S. Li, M. Yu, X. He, T.A. White, X. Liang, Highly active and selective Cu-ZnO based catalyst for methanol and dimethyl ether synthesis via CO_2 hydrogenation, Fuel, 239 (2019) 1125-1133.

[71] Dimethyl ether synthesis from CO_2 hydrogenation on La-modified CuO-ZnO-Al_2O_3/HZSM-5 bifunctional catalysts, Journal of Rare Earths, 31 (2013) 470.

[72] F. Zha, J. Ding, Y. Chang, J. Ding, J. Wang, J. Ma, Cu–Zn–Al Oxide Cores Packed by Metal-Doped Amorphous Silica–Alumina Membrane for Catalyzing the Hydrogenation of Carbon Dioxide to Dimethyl Ether, Industrial & Engineering Chemistry Research, 51 (2011) 345-352.

[73] G.Qi, J.Fei., X. Zheng, Z. Hou,DME synthesis from carbon dioxide and hydrogen, Catal Let. 72 (2001) 1-2.

Chapter 6

CONCLUSION AND OUTLOOK

Over the past centuries, CO_2 emissions have increased in an unprecedented rate by the burning fossil fuels. CO_2 is one of the main players of the greenhouse gases emitted from human operations into the Earth's atmosphere. The growing quantity of greenhouse gasses generated over the centuries by human civilization has an adverse effect on climate change. Therefore, the reduction of CO_2 concentration in the atmosphere has become a main target globally. The chemical conversion of CO_2 not only mitigates atmospheric CO_2 emissions into the Earth's environment but also generates carbon compounds that can be used as precursors for chemical and fuel manufacturing. In this respect, CO_2 hydrogenation is a powerful and feasible method. Production of DME from CO_2 hydrogenation has been received a considerable attention in the recent years as a potential diesel fuel replacement used in combustion engines. Extensive works have been carried out to enhance the techniques of DME synthesis and the catalysts. Therefore, this thesis focuses on development of an efficient catalyst for the conversion of CO_2 into DME.

In this thesis, the direct hydrogenation of CO_2 to DME has been studied in a single-pass fixed-bed reactor. For this purpose, a homemade high-pressure flow reactor system was designed equipped with Micro GC which was calibrated for all hydrogenation products. CO_2 hydrogenation reaction carried out under a suitable temperature and pressure of 250 °C, 45 bar and the appropriate gas hourly space velocity of 40 000 mL CO_2 g_{cat}^{-1} h^{-1} with a feed ratio of H_2:CO_2 = 3:1. A homemade MCM-41 supported heteropoly acid (tungstophosphoric acid) catalyst in a physical addition to commercially available CuO-ZnO-Al_2O_3 were used as the catalysts. Detailed characterization of both metal catalyst CuO-ZnO-Al_2O_3 and acid catalyst TPA/MCM-41 catalysts were performed by conducting XRD, NH_3-TPD, FTIR, BET analysis methods. The catalytic behavior of the mixed CuO-ZnO-Al_2O_3 (MSC) and TPA/MCM-41(SAC) catalysts has been assessed, considering the influence of temperature (220-250 °C), gas hourly space velocity (7000-40 000 mL CO_2 g_{cat}^{-1} h^{-1}), different metallic and acidic mixing

ratio (MSC: SAC= 2:1, 3:1, 4:1(wt:wt)), finally different TPA loading on MCM-41 (weight ratio of 30:70, 40:60, 60:40, 80:20 (wt:wt)) on the activity-selectivity pattern. The results disclosed that the highest DME space time yield was achieved at a TPA loading of 60 wt% in the TPA/MCM-41 catalyst and at a CuO-ZnO-Al_2O_3:TPA/MCM-41 mixing ratio of 4:1 using a gas hourly space velocity of 40 000 mL CO_2 g_{cat}^{-1} h^{-1} with an H_2:CO_2 ratio of 3:1 at 250 °C and 45 bar. Consequently, under these conditions DME production rate of 1551.5 g $_{DME}$ $kg_{cat}^{-1}h^{-1}$ was obtained. To the best of our knowledge, this value of DME production rate is the highest ever reported for single-pass DME production from CO_2 hydrogenation.

In conclusion, heteropoly acids are very promising materials as an acid catalyst for direct CO_2-to-DME synthesis. Here we put the potential of heteropoly acid catalysts which was mixed with the commercial methanol synthesis catalyst for the production of DME. CO_2 hydrogenation process is very popular topic for both academia and industry. Therefore, there are many things to do as the future work that are briefly discussed below:

Using special design metal catalysts for CO_2 hydrogenation: It is important to note that, here, to be able to a assess the potential ofacid catalyst activity, we used an ordinary commercial methanol synthesis catalyst, CuO-ZnO-Al_2O_3, for CO_2 activation to produce methanol. It's very well-known and catalytic properties are well-documented for this reaction as well, however this catalyst is designed for CO hydrogenation not for CO_2 conversion. Therefore, specially design catalysts for CO_2 hydrogenation are needed. For example, it is known that CuO and ZrO_2 have very great metal support interaction from the literature. Modification of CuO based catalyst which exhibits a high degree of synergistic effect can be good candidate for using promoters to improve the catalytic performance. Because of the thermodynamics point of view, it is hard to activate the CO_2. The promoters can boost the absorption of CO_2 on catalyst surface and H_2 dissociation, so CO_2 conversion can be enhanced. Also, for CuO-based catalyst, CuO particle size can be a parameter for catalytic activity. In preparation step by playing with calcination temperature, different particle size of CuO catalysts can be synthesized and their catalytic performances can be studied for CO_2 hydrogenation reaction. Apart from the CuO-based catalyst, there is an increasing trend for using oxygen deficient metal oxides on which CO_2 activation is more favorable and they can give nearly 100% selectivity to MeOH, so they can be studied as a future work. In addition to these, for this reaction the main challenge is deal with produced water during reaction, it causes deactivation

of catalyst. Therefore, use of hydrophobic catalyst or *in-situ* removal of water from reaction can enhance the activity, selectivity of the catalyst which can be stable over time.

Using different HPAs as an acid catalyst: In this study**,** we only used one type of heteropoly acid which is tungstophosphoric acid. However, among the wide range of Keggin-type heteropoly acids, tungstosilicic acid ($H_4SiW_{12}O_{40}$) molybdophosphoric acid ($H_3PMo_{12}O_{40}$), are also commercially available and their all redox and acid properties different from each other and their chemical composition can be tuned as well. According to their different acidic strength, they can exhibit different catalytic activity. Therefore, to able to see the potential of the heteropoly acid family, they can be used on different supports to investigate their performance on CO_2-to-DME.

Considering the effect of proximity of metal and acid sites and catalyst bed configuration: In this work, we mixed acid and metal catalyst physically. However, it is known that from literature, catalytic activity can be affected by the integration manner of the active components. For example, it can be tried shortening the distance between the components by preparing a powder mixture or pelleting of two components then grinding to examine the effect of intimate contact. Even it can be separated these two components in the reactor by preparing dual bed first with acid component packed below metal component and separated by quartz wool. Apart from the acid and metal function proximity, even proximity of metallic function components (Cu-Zn for our case) can be examined since proximity of adsorption sites might affect the catalytic performance.

Chapter A1

CONVERSION OF CO_2 INTO DIMETHYL ETHER ON A PHYSICAL MIXTURE OF TPA/MCM-41 AND CuO-ZnO-Al_2O_3

In this part the commercial methanol synthesis catalyst's (MSC), CuO-ZnO-Al_2O_3 (Alfa Aesar product no. 45776) characterization is presented.

A1.1 Catalyst Characterization Methods

A1.1.1 Thermogravimetric Analysis (TGA)

TGA analysis was studied by Perkin Elmer TGA 4000 model instrument. Before the sample loading Platinum pans were used and tared. TGA analyses of approximately 25 mg of sample was performed. First, sample was heated to 150 °C under nitrogen flow with a temperature ramp of 5 °C min^{-1} waited 1 h under that conditions. After 1 h, sample was cooled to room temperature under same flow. Then, temperature was then increased up to 800 °C by a heating rate of 2 °C min^{-1}.

A1.1.2 X-Ray Fluorescence (XRF)

Elemental composition was measured by a Bruker S8 Tiger XRF Spectrometer in standardless mode working under He atmosphere with a 18 mm mask. Sample was loaded in to a sample cup with a thin film support (Prolene film with 4µm thickness). A 4 KW, Rh anode X-ray tube was used to generate X-rays for the measurement. SpectraPlus Eval2 V2.2.454 was used to interpret data.

A1.1.3 X-Ray Diffraction (XRD)

A Bruker D8 Discover X-Ray Diffraction instrument was used with a Cu Kα1 radiation source with an employed wavelength of 1.5418 Å for XRD analysis. Power rating values of instrument were 40 kV and 40 mA. To detect diffracted X-rays, 1D detector (Vantec-1) was used and divergence slit was set to 1 mm. The range between 10-90° with step size 0.01263° was used for 2Θ value. XRD samples were prepared by approximately 10 mg of catalyst was placed on double sided tape which was attached to glass slide. Then, the glass side was put on sample holder. For phase definition, ICDD PDF-4 2018 database was used by subtracting the background.

A1.1.4 Brunauer-Emmett-Teller (BET) and Barrett-Joyner-Halenda (BJH) analyses

Using BET and BJH analyses, surface area and pore volume of sample were recorded using a Micrometrics ASAP 2020 physisorption analyzer at liquid nitrogen temperature -196 °C. For each experiment 0.5 g samples were degassed at 200 °C for 12 h.

A1.1.5 Temperature Programmed Reduction with Hydrogen (H_2-TPR)

AutoChem II 2920 instrument was employed for TPR analysis. Approximately 0.1 g sample was placed in U-shape quartz reactor. For drying part, sample was heated to 160 °C under helium flow (50 ml min^{-1}) with a temperature ramp of 5 °C min^{-1}. The sample was hold 1 h at 160 °C under the mentioned flow. After 1 h, sample was cooled to room temperature under same flow. After drying, sample was heated to 700 °C reached with a Temperature ramp of 5 °C min^{-1} under 10%H_2-Argon mixture. The effluent gas stream was recorded by TCD signals. Using the Origin Lab software, the spectrum of H_2-TPR was deconvoluted and calculated corresponding areas.

A1.1.6 Temperature Programmed Desorption with Hydrogen (H_2-TPD)

A Micrometrics AutoChem II 2920 instrument equipped with a thermal conductivity detector and an MKS Cirrus 2 mass spectrometer was used to perform H_2- TPD measurements.

Approximately 0.1 g of catalysts were loaded U-shaped quartz microreactor for measurement. Catalysts were pretreated at 160 °C for 1 h under helium flow. After 1 h, sample was cooled to room temperature under same flow. The catalyst was first reduced at 300 °C for 2 h in a flow of 10% H_2-Ar (50 ml min^{-1}) by temperature ramp 5°C min^{-1}. After cooling down to 50 °C, the catalyst was saturated with pure 10% H_2-Ar (50 ml min^{-1}) at 50 °C, for 1 h and then flushed with helium to remove the physical adsorbed molecules then started to record TCD signals. Under helium flow, sample were heated up to 700 °C with a ramp rate of 5 °C min^{-1} while exit gas was monitored by TCD signals. Using the Origin Lab software, the spectrum of H_2-TPD was deconvoluted and calculated corresponding areas.

A1.1.7 Temperature Programmed Desorption with Ammonia (NH_3-TPD)

A Micrometrics AutoChem II 2920 instrument equipped with a thermal conductivity detector and an MKS Cirrus 2 mass spectrometer was used to perform NH_3- TPD measurements. Approximately 0.17 g of catalysts were loaded U-shaped quartz microreactor for measurement. Catalysts were pretreated at 250 °C for 2 h under helium flow (50 cm^3 min^{-1}). Then, they were introduced to NH_3 flow (50 cm^3 min^{-1}) at 40 °C for 1 h. Excess NH_3 was removed for 1 h at 100 °C under helium flow. Sample was heated up to 700 °C with a ramp rate of 3 °C min^{-1} while exit gas was monitored by TCD signals. Using the Origin Lab software, the spectrum of NH_3-TPD was deconvoluted and calculated corresponding areas under the curves to quantify the acid amount using calibrated TCD signals.

A1.1.8 Temperature Programmed Desorption with Nitrogen (N_2-TPD)

A Micrometrics AutoChem II 2920 instrument equipped with a thermal conductivity detector and an MKS Cirrus 2 mass spectrometer was used to perform N_2- TPD measurements. Approximately 0.23 g of catalysts were loaded U-shaped quartz microreactor for measurement. Sample was heated up to 800 °C with a ramp rate of 2 °C min^{-1} under nitrogen flow (50 ml min^{-1}) while exit gas was monitored by TCD signals. Using the Origin Lab software, the spectrum of N_2-TPD was deconvoluted and calculated corresponding areas.

A1.2 Catalyst Characterization Results and Discussion

A1.2.1 Thermogravimetric Analysis (TGA)

Thermal stability of commercial CuO-ZnO-Al_2O_3 catalyst was analyzed by TGA. Figure A1.1 showed the results of the TGA measurement.

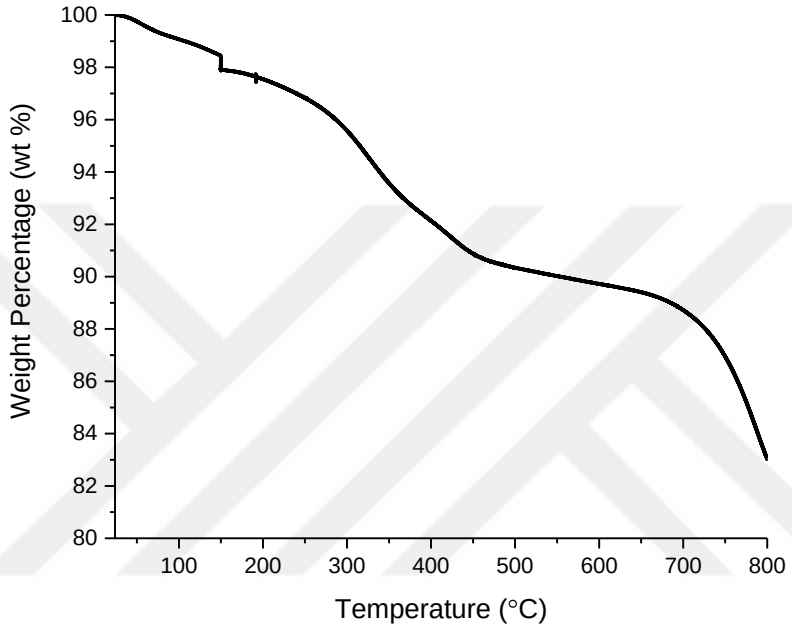

Fig. A1.1 TGA analysis of commercial CuO-ZnO-Al_2O_3.

According to the TGA result, the thermal decomposition of the commercial methanol catalyst takes place in three steps. In the first stage, the decomposition which occurs until the drying process at 150 °C belongs to the removal of the water which is physically attached to the surface of the catalyst. Two further peaks are observed at 275 °C and 725 °C where thermal degradation occurs.

A1.2.2 X-Ray Fluorescence (XRF)

Chemical composition of CuO-ZnO-Al_2O_3 obtained by XRF are provided in Table A1.1. Both the elemental composition and the element oxides of the sample were determined as weight percent (%).

Table A1.1 Chemical composition of the commercial CuO-ZnO-Al_2O_3.

Oxides	Weight %	Elements	Weight %
CuO	64.1	Cu	67.3
ZnO	25.6	Zn	26.1
Al_2O_3	9.05	Al	5.8
MgO	1.25	Mg	0.8

A1.2.3 X-Ray Diffraction (XRD)

Fig. A1.2 presents the XRD patterns of CuO-ZnO-Al_2O_3 catalyst from 2θ = 10 to 90°.

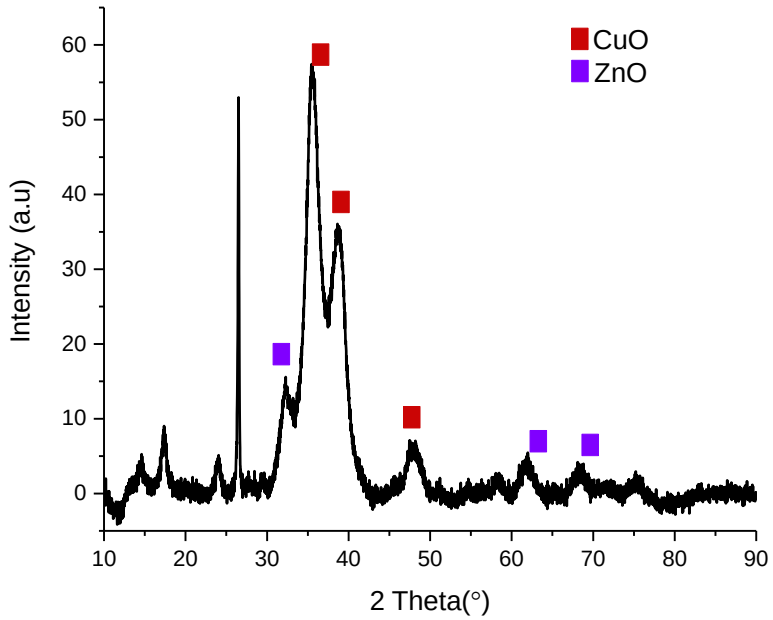

Fig. A1.2 XRD pattern of commercial CuO-ZnO-Al_2O_3.

According to the database, the signals of CuO are 2θ = 35.51 °, 38.96 °, 48.31 ° (PDF 00-048-1548). The signals of ZnO are defined as 2θ = 32.50 °, 62.54 °, 68.71 ° [1].

A1.2.4 Brunauer-Emmett-Teller (BET)

BET analysis of CuO-ZnO-Al_2O_3 catalyst was also carried out. Results were shared in Table A1.2 and showed in Fig. A1.3.

Table A1.2 BET analyses of the commercial CuO-ZnO-Al_2O_3.

BET surface area	106 m^2 g^{-1}
Langmuir surface area	172 m^2 g^{-1}
BJH Adsorption cumulative volume of pores	0.18 cm^3 g^{-1}
BJH Desorption cumulative volume of pores	0.2 cm^3 g^{-1}
BJH Adsorption average pore diameter	7.2 nm
BJH Desorption average pore diameter	6.3 nm

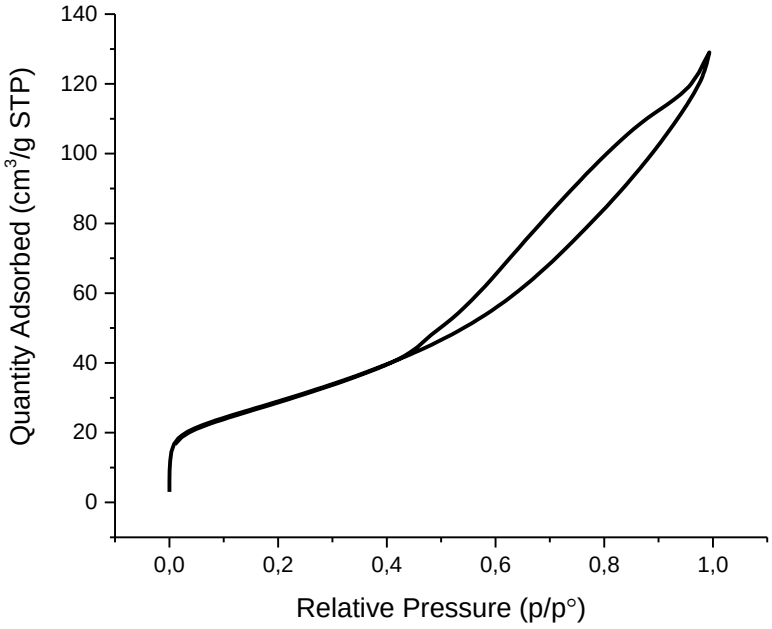

Fig. A1.3 N_2 adsorption and desorption isotherms of commercial CuO-ZnO-Al_2O_3.

As shown in Fig. A1.3, CuO ZnO-Al_2O_3 catalyst is compatible with Type-IV according to adsorption isothermal types. Type-IV adsorption generally shows the pore structure in the form of an ink bottle. As given in Table A1.2, it reveals meso porous structure with an average pore diameter of 7 nm. Also, as can be seen in Fig. A1.3, adsorption and desorption isotherms followed by different paths, so it generated adsorption hysteresis.

A1.2.5 Temperature Programmed Reduction with Hydrogen (H_2-TPR)

The reduction behavior of the commercial methanol synthesis was studied by H_2-TPR. The corresponding reduction profiles are shown in Fig. A1.4 and Fig. A1.5.

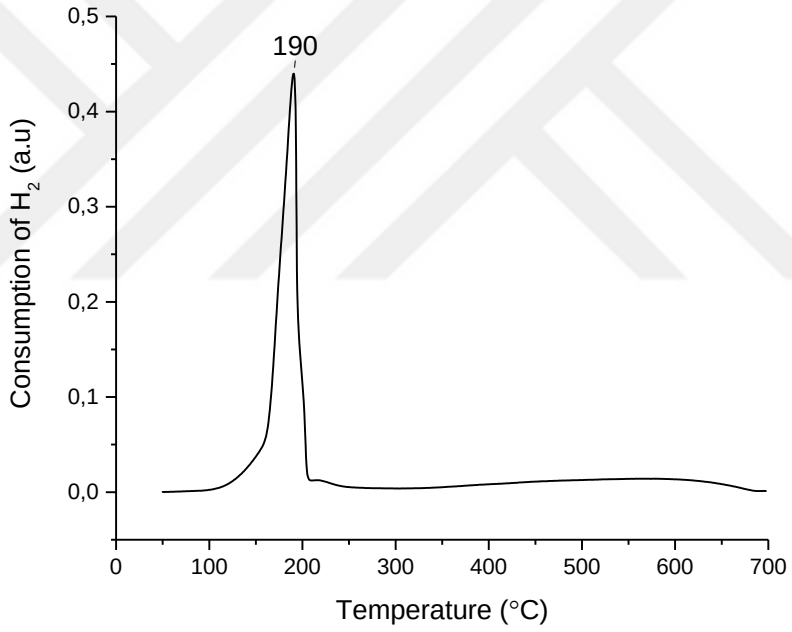

Fig. A1.4 TPR patterns of commercial CuO-ZnO-Al_2O_3.

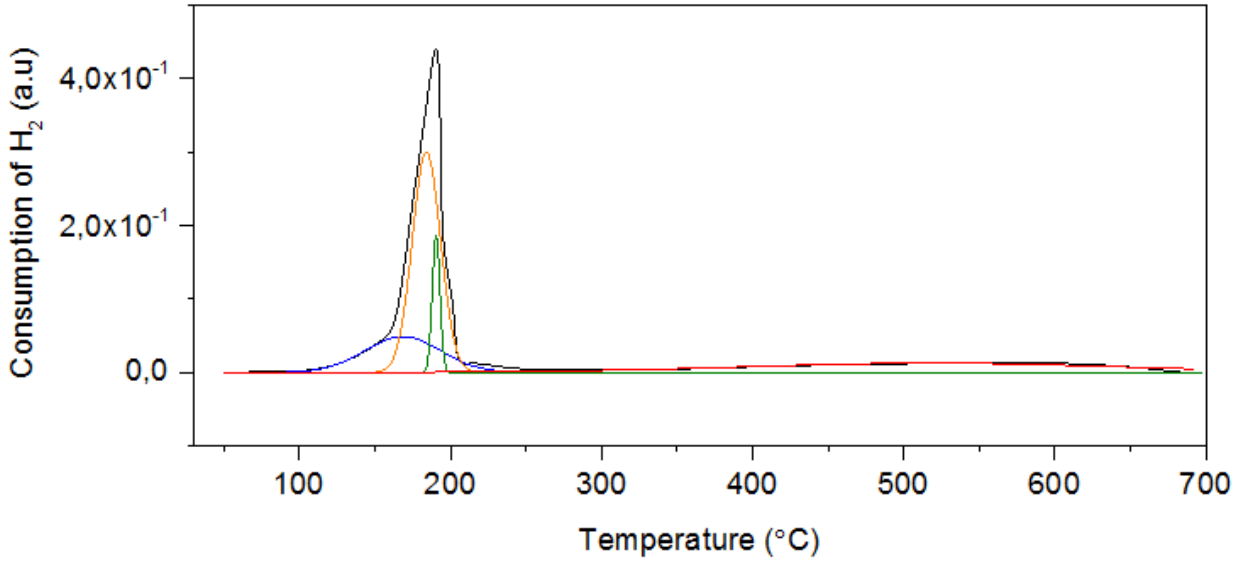

Fig. A1.5 Detailed analysis of TPR patterns of commercial CuO-ZnO-Al_2O_3 (the separated peaks are given in different colors).

The reduction behavior of commercial methanol synthesis catalyst between 50-700 °C was investigated, and the reduction temperature of CuO under the above conditions was observed with a sharp peak formation at 190 °C in Fig A1.4 [2]. Due to the high thermal stability of ZnO, it gives a large and quite small peak at about 518 °C in the TPR analysis [3, 4]. Detailed analysis of the reduction process in Fig. A1.5 shows that the hydrogen consumption curves are divided into multiple sections. Here, the peak of low temperature at 168 °C indicates highly dispersed CuO, while the peaks at 184 °C and 190 °C correspond to the reduction in bulk CuO [5].

A1.2.6 Temperature Programmed Desorption with Hydrogen (H_2-TPD)

H_2–TPD was also studied. H_2–TPD pattern is shown in Fig. A1.6 while quantitative data are reported in Table A1.3.

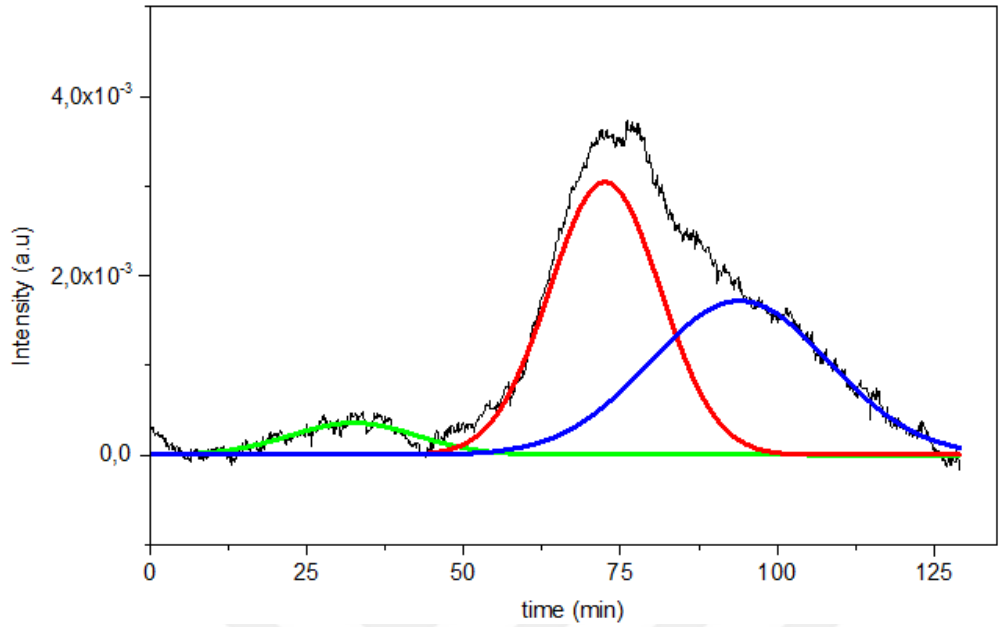

Fig. A1.6 Detailed analysis of H_2-TPD patterns of commercial CuO-ZnO-Al_2O_3 (the separated peaks are given in different colors which indicate green: α; red: β^1; blue: β^2 peaks).

Table A1.3 The maximum temperature and H_2 desorption amount over commercial CuO-ZnO-Al_2O_3.

Peak α		**Peak β (β^1 and β^2)**	
Temperature (°C)	H_2 desorption (μmol g^{-1})	Temperature (°C)	H_2 desorption (μmol g^{-1})
198	246.8	409 - 497	3498.6

As shown in Fig. A1.6, the H_2-TPD curve of the catalyst shows the two main hydrogen desorption peaks that combine at about 198 ° C and 409 and 497 ° C. According to the literature, the peak at low temperature corresponds to the desorption of atomic hydrogen in the copper regions and the broad peak at high temperature corresponds to the desorption of strongly

adsorbed hydrogen at the ZnO surface [6]. Al_2O_3 does not adsorb hydrogen and therefore it does not affect the adsorption of hydrogen in other regions [7].

A1.2.7 Temperature Programmed Desorption with Ammonia (NH_3-TPD)

The NH_3-TPD of the CuO-ZnO-Al_2O_3 was measured to determine the surface acidity which shown in Fig.A1.7.

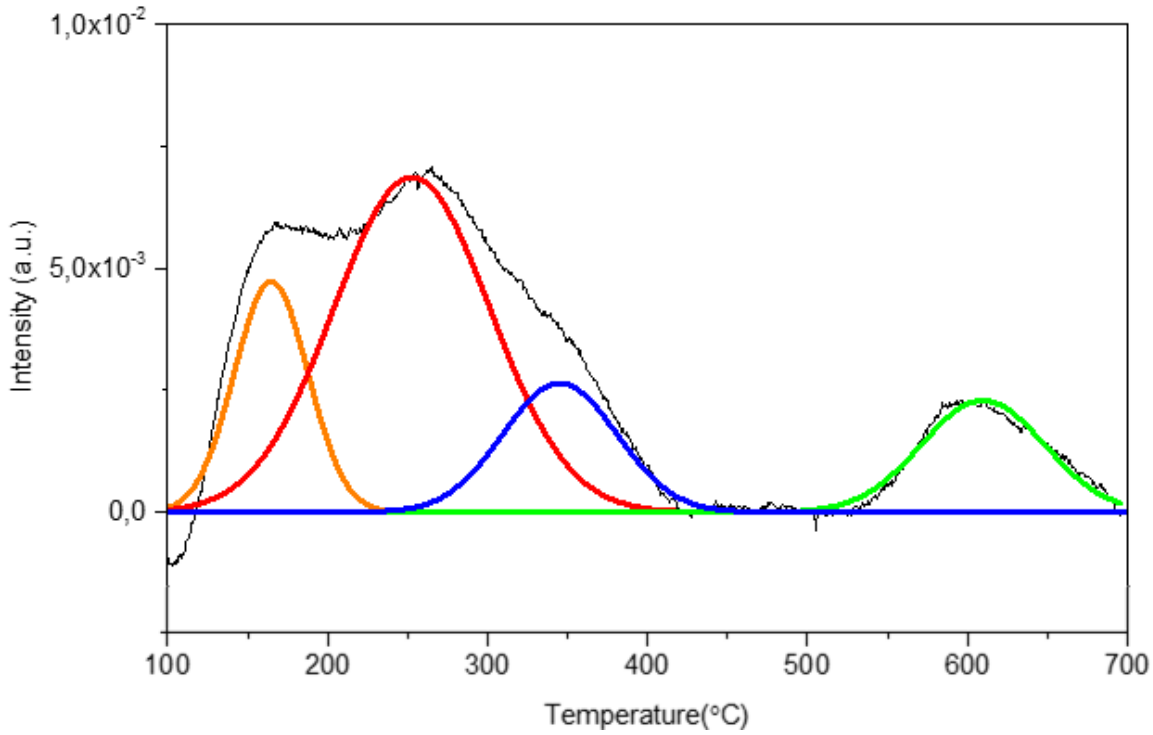

Fig. A1.7 NH_3-TPD patterns of commercial CuO-ZnO-Al_2O_3.

The NH_3-TPD curve in Fig. A1.7 shows the adsorption peaks which are indicating the presence of weak, moderate, strong acid sites on catalyst surface. NH_3 adsorption in Lewis acid sites is stronger than Brønsted acid sites [8]. Accordingly, the low temperature adsorption peaks indicate the Brønsted acid sites, while the high temperature peak belongs to the Lewis acid sites. Desorption peaks of weak acid site at 164 °C and 252 °C which may be ascribed to the Brønsted acid sites obtained from surface hydroxyl groups in ZnO or Al_2O_3 and Lewis acid sites are obtained from the cations of Al-O-M^{2+} (M = Zn, Cu) species [9].

A1.2.8 Temperature Programmed Desorption with Nitrogen (N_2-TPD)

The thermal decomposition of the commercial methanol synthesis catalyst under nitrogen gas flow was investigated which is shown in Fig. A1.8

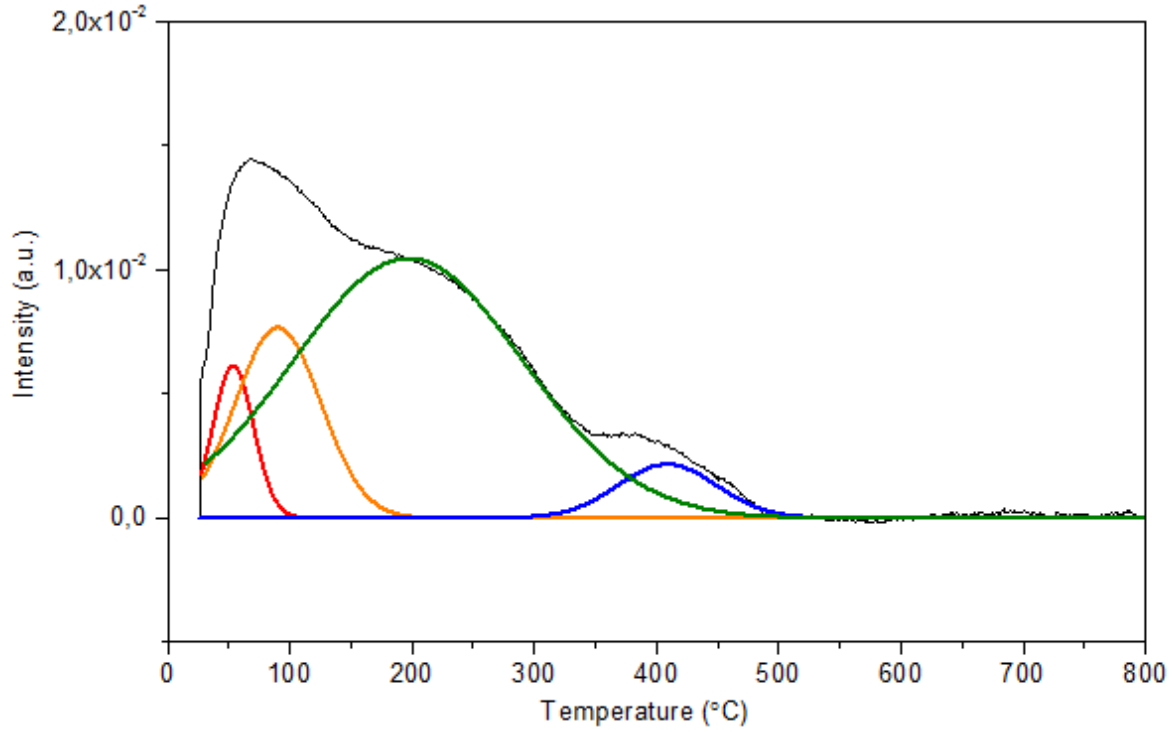

Fig. A1.8 N_2-TPD patterns of commercial CuO-ZnO-Al_2O_3.

When thermal decomposition of the commercial methanol catalyst under nitrogen gas flow is examined according to Fig. A1.8 by N_2-TPD, peaks formation are observed at temperatures of 53, 90, 196, and 408 °C. The first two peaks formed at low temperatures correspond to the physically adsorbed water molecules.

References

[1] O. Martin, A.J. Martin, C. Mondelli, S. Mitchell, T.F. Segawa, R. Hauert, C. Drouilly, D. Curulla-Ferre, J. Perez-Ramirez, Indium Oxide as a Superior Catalyst for Methanol Synthesis by CO2 Hydrogenation, Angew Chem Int Ed Engl, 55 (2016) 6261-6265.

[2] F. Frusteri, M. Cordaro, C. Cannilla, G. Bonura, Multifunctionality of Cu-ZnO-ZrO_2/H-ZSM5 catalysts for the one-step CO_2-to-DME hydrogenation reaction, Applied Catalysis B: Environmental, 162 (2015) 57-65.

[3] M. Liang, W. Kang, K. Xie, Comparison of reduction behavior of Fe_2O_3, ZnO and $ZnFe_2O_4$ by TPR technique, Journal of Natural Gas Chemistry, 18 (2009) 110-113.

[4] M.A. Valenzuela, Preparation, characterization and photocatalytic activity of ZnO, Fe_2O_3 and $ZnFe_2O_4$, Journal of Photochemistry and Photobiology A: Chemistry 148 (2002) 177–182

[5] P. Gao, F. Li, L. Zhang, N. Zhao, F. Xiao, W. Wei, L. Zhong, Y. Sun, Influence of fluorine on the performance of fluorine-modified Cu/Zn/Al catalysts for CO_2 hydrogenation to methanol, Journal of CO_2 Utilization, 2 (2013) 16-23.

[6] P. Gao, H. Yang, L. Zhang, C. Zhang, L. Zhong, H. Wang, W. Wei, Y. Sun, Fluorinated Cu/Zn/Al/Zr hydrotalcites derived nanocatalysts for CO_2 hydrogenation to methanol, Journal of CO_2 Utilization, 16 (2016) 32-41.

[7] P. Gao, F. Li, H. Zhan, N. Zhao, F. Xiao, W. Wei, L. Zhong, H. Wang, Y. Sun, Influence of Zr on the performance of Cu/Zn/Al/Zr catalysts via hydrotalcite-like precursors for CO_2 hydrogenation to methanol, Journal of Catalysis, 298 (2013) 51-60.

[8] J.I. Di Cosimo, Apesteguı, C.R.´a, M.J.L. Ginés, E. Iglesia, Structural Requirements and Reaction Pathways in Condensation Reactions of Alcohols on Mg_yAlO_x Catalysts, Journal of Catalysis, 190 (2000) 261-275.

[9] C. Zhang, H. Yang, P. Gao, H. Zhu, L. Zhong, H. Wang, W. Wei, Y. Sun, Preparation and CO_2 hydrogenation catalytic properties of alumina microsphere supported Cu-based catalyst by deposition-precipitation method, Journal of CO_2 Utilization, 17 (2017).